AMERICAN SOCIETY FOR MICROBIOLOGY | Journal of Virology®

VIRUS-CELL INTERACTIONS

Hepatitis C Virus Replication Depends on Endosomal Cholesterol Homeostasis

Ina Karen Stoeck,[a] Ji-Young Lee,[a] Keisuke Tabata,[a] Inés Romero-Brey,[a] David Paul,[a]* Philipp Schult,[a] Volker Lohmann,[a] Lars Kaderali,[b] Ralf Bartenschlager[a]

[a]Department of Infectious Diseases, Molecular Virology, Heidelberg University, Heidelberg, Germany
[b]Institute of Bioinformatics, University Medicine Greifswald, Greifswald, Germany

ABSTRACT Similar to other positive-strand RNA viruses, hepatitis C virus (HCV) causes massive rearrangements of intracellular membranes, resulting in a membranous web (MW) composed of predominantly double-membrane vesicles (DMVs), the presumed sites of RNA replication. DMVs are enriched for cholesterol, but mechanistic details on the source and recruitment of cholesterol to the viral replication organelle are only partially known. Here we focused on selected lipid transfer proteins implicated in direct lipid transfer at various endoplasmic reticulum (ER)-membrane contact sites. RNA interference (RNAi)-mediated knockdown identified several hitherto unknown HCV dependency factors, such as steroidogenic acute regulatory protein-related lipid transfer domain protein 3 (STARD3), oxysterol-binding protein-related protein 1A and -B (OSBPL1A and -B), and Niemann-Pick-type C1 (NPC1), all residing at late endosome and lysosome membranes and required for efficient HCV RNA replication but not for replication of the closely related dengue virus. Focusing on NPC1, we found that knockdown or pharmacological inhibition caused cholesterol entrapment in lysosomal vesicles concomitant with decreased cholesterol abundance at sites containing the viral replicase factor NS5A. In untreated HCV-infected cells, unesterified cholesterol accumulated at the perinuclear region, partially colocalizing with NS5A at DMVs, arguing for NPC1-mediated endosomal cholesterol transport to the viral replication organelle. Consistent with cholesterol being an important structural component of DMVs, reducing NPC1-dependent endosomal cholesterol transport impaired MW integrity. This suggests that HCV usurps lipid transfer proteins, such as NPC1, at ER-late endosome/lysosome membrane contact sites to recruit cholesterol to the viral replication organelle, where it contributes to MW functionality.

IMPORTANCE A key feature of the replication of positive-strand RNA viruses is the rearrangement of the host cell endomembrane system to produce a membranous replication organelle (RO). The underlying mechanisms are far from being elucidated fully. In this report, we provide evidence that HCV RNA replication depends on functional lipid transport along the endosomal-lysosomal pathway that is mediated by several lipid transfer proteins, such as the Niemann-Pick type C1 (NPC1) protein. Pharmacological inhibition of NPC1 function reduced viral replication, impaired the transport of cholesterol to the viral replication organelle, and altered organelle morphology. Besides NPC1, our study reports the importance of additional endosomal and lysosomal lipid transfer proteins required for viral replication, thus contributing to our understanding of how HCV manipulates their function in order to generate a membranous replication organelle. These results might have implications for the biogenesis of replication organelles of other positive-strand RNA viruses.

KEYWORDS HCV, RNA replication, DMV, cholesterol, NPC1, lipid transfer

Received 13 July 2017 **Accepted** 28 September 2017

Accepted manuscript posted online 18 October 2017

Citation Stoeck IK, Lee J-Y, Tabata K, Romero-Brey I, Paul D, Schult P, Lohmann V, Kaderali L, Bartenschlager R. 2018. Hepatitis C virus replication depends on endosomal cholesterol homeostasis. J Virol 92:e01196-17. https://doi.org/10.1128/JVI.01196-17.

Editor Julie K. Pfeiffer, University of Texas Southwestern Medical Center

Address correspondence to Ralf Bartenschlager, ralf.bartenschlager@med.uni-heidelberg.de.

* Present address: David Paul, MRC Laboratory of Molecular Biology, Cambridge, United Kingdom.

At present, around 70 million people are infected with hepatitis C virus (HCV) and at risk to develop severe liver damage, including liver fibrosis, cirrhosis, and hepatocellular carcinoma (1). Due to the lack of a prophylactic vaccine and the restricted access of patients to potent but costly direct-acting antiviral drugs (DAAs), HCV is far from being eradicated and will remain a global health burden for many years (2). HCV belongs to the *Hepacivirus* genus within the family *Flaviviridae* and is characterized by a single-stranded RNA genome of positive polarity. The concerted action of 10 viral proteins orchestrates the HCV life cycle. These include core, E1, and E2, the main constituents of the virion, which assembles with the help of p7, nonstructural protein 2 (NS2), and the replicase proteins NS3, -4A, -4B, -5A, and -5B (3). Similar to other positive-strand RNA viruses, HCV causes profound membrane rearrangements, designated the membranous web, in infected cells (4, 5). This replication organelle (RO) is most likely derived from the endoplasmic reticulum (ER) and composed of single-, double- and multimembrane vesicles (6). The double-membrane vesicles (DMVs) are the most abundant membrane structures present in HCV-infected cells, and the kinetics of their appearance correlates with the kinetics of viral RNA replication (6). In addition, affinity-purified DMVs were shown to contain enzymatically active viral RNA replicase, supporting the assumption of DMVs being the site of HCV RNA replication (7).

The molecular details of the generation of the HCV RO are far from being elucidated fully, but it involves the concerted action of host and viral factors (8). Indeed, there is increasing evidence that HCV and other positive-strand RNA viruses usurp cellular proteins and specific lipid species to create a microenvironment supporting viral RNA replication (4, 9). For instance, HCV RNA replication has been reported to occur in association with detergent-resistant membranes, believed to be enriched in unesterified/free cholesterol and sphingolipids (10, 11). In agreement with this, unesterified cholesterol was shown to be a major structural component of the HCV RO (7). Considering that the ER, despite being the site of *de novo* cholesterol synthesis, has a low cholesterol content (12), the HCV RO has to acquire unesterified membrane cholesterol either by on-site *de novo* synthesis of this lipid or by directed cholesterol transport to the RO. Consistently, HCV has been reported to hijack the function of the oxysterol-binding protein (OSBP) (13, 14). In uninfected cells, OSBP catalyzes the transfer of unesterified cholesterol from the ER to the Golgi compartment, presumably by exchanging cholesterol for phosphatidylinositol-4-phosphate (PI4P), which is present at its highest concentration in the Golgi apparatus and at its lowest concentration in the ER (15). To enrich for cholesterol at its (ER-derived) RO, HCV has been proposed to exploit the OSBP-mediated PI4P-cholesterol countertransport (14; reviewed in reference 5). By recruiting and activating cellular PI4P kinase III alpha (PI4KIIIA), HCV causes a local accumulation of PI4P at RO membranes (16, 17), which is assumed to drive the release of cholesterol from OSBP in exchange for PI4P (14). Besides OSBP, another PI4P-interacting lipid transfer protein (LTP), the glycosphingolipid transfer protein four-phosphate adaptor protein 2 (FAPP2), has been reported to be involved in a similar manner in the HCV replication cycle (18). These observations illustrate that both the biogenesis and the activity of the viral RO appear to depend on several host cell factors regulating the access to lipids. In the present study, we used an RNA interference (RNAi)-based approach to determine the importance of LTPs implicated in sterol transfer for the HCV replication cycle in comparison to that of the closely related dengue virus (DENV). We focused on direct lipid transfer at membrane contact sites of the ER with other organelles, such as the plasma membrane (PM), the late endosome (LE), and the lysosome (LY), and assessed the impact of impaired cholesterol transport on HCV RO integrity.

RESULTS

HCV RNA replication depends on the function of lipid transfer proteins. Several recent findings point to an active exploitation of LTPs by HCV in order to enrich specific lipid species at its sites of genome replication (14, 18). While the main focus so far has been on OSBP mediating cholesterol transport at ER-Golgi contact sites, here we aimed

to identify additional LTPs important for the replication cycle of HCV. These comprised members of the OSBP-related/like protein (ORP/OSBPL) family (19) that might share redundant functions with OSBP, members of the steroidogenic acute regulatory protein-related lipid transfer (START) domain (STARD) family (20), and other lipid transport factors, such as the Niemann-Pick type C1 and C2 proteins (NPC1 and NPC2, respectively) (21–23) (Fig. 1A). To assess their involvement in the HCV replication cycle, we analyzed the effect of gene knockdown of each candidate on the complete viral replication cycle by using a fully functional *Renilla* luciferase reporter virus and compared it to the phenotypes obtained with the closely related DENV (Fig. 1A). As technical controls, small interfering RNAs (siRNAs) targeting the established HCV host dependency factors PI4KIIIA (17) and ApoE (24) were included, in addition to an siRNA targeting the *Renilla* luciferase gene present in the genomes of both reporter viruses. All controls reduced virus titers profoundly, indicating the robustness of the RNAi screen (Fig. 1B, gray bars). Under these conditions, we identified STARD3, PITPNM1, OSBPL3, and NPC1 as novel host dependency factors and OSBPL1A and -B (two isoforms of ORP1; also known as ORP1S and ORP1L, respectively) and COL4A3BP as inhibitory factors selectively affecting HCV but not DENV (Fig. 1B, red bars). In line with earlier reports (13, 14), knockdown of OSBP caused only a moderate reduction of HCV particle production (Fig. 1B).

With the aim of characterizing the role of lipid transfer at membrane contact sites other than the Golgi-ER interface for HCV replication, we focused on STARD3 and NPC1, described to promote the egress of unesterified cholesterol from late endosomal (LE)/lysosomal (LY) compartments (22, 25), and ORP1, isoform OSBPL1B (ORP1L), thought to regulate the establishment of ER-LE/LY membrane contact sites (26) (Fig. 1C). Knockdown of either one of the candidates by use of short hairpin RNA (shRNA), used to validate the primary screen results, reduced entry/replication of HCV (Fig. 1D, left panel), with no discernible additional impact on assembly/release of infectious particles (note that the lower virus titer correlated well with reduced RNA replication) (Fig. 1D, middle panel). Importantly, knockdown of PI4KIIIA or ApoE impaired early or late events of the viral replication cycle, respectively (Fig. 1D, left and middle panels), consistent with their role in RNA replication or production of infectious particles (17, 24), thus confirming the quality of the assay. Only one of the two shRNAs targeting STARD3 diminished cell viability, while all the other shRNAs were well tolerated (Fig. 1D, right panel). These results argue for an important role of LTPs at the ER-LE/LY membrane contact sites for HCV replication.

Predominant role of NPC1 in HCV RNA replication. Among all the candidates tested, knockdown of NPC1 expression caused the most profound and robust phenotype, as two different shRNAs substantially reduced viral entry/replication in two different cell lines tested, with minor effects on cell viability (Fig. 1D, left and right panels). Therefore, we focused our further analysis on this LTP.

NPC1 is a transmembrane protein localized to the limiting membrane of LE, where it contributes to the export of low-density lipoprotein (LDL)-derived unesterified cholesterol (Fig. 1C) (22). Moreover, this protein has been reported to be involved in Ebola virus entry by promoting viral escape from LE compartments (27). Given our previous results indicating that NPC1 was involved in either viral entry or RNA replication, we bypassed the entry step by using stable subgenomic reporter replicons, thus selectively analyzing the impact of NPC1 knockdown on HCV RNA replication (Fig. 2A). We found that knockdown of NPC1 expression reduced the replication of subgenomic luciferase reporter replicons stably replicating in Huh7 cells (Fig. 2A and B). Interestingly, the magnitude of the reduction appeared to depend on the genotype or the replication capacity of the isolate, which is exceptionally high in the case of the JFH1 isolate but much lower with the Con1 isolate (28, 29).

To confirm the important role of NPC1 in HCV RNA replication, we used two alternative approaches. The first one was knockout (KO) of the NPC1 gene by use of the clustered regularly interspaced short palindromic repeat (CRISPR)/Cas9 system. To this

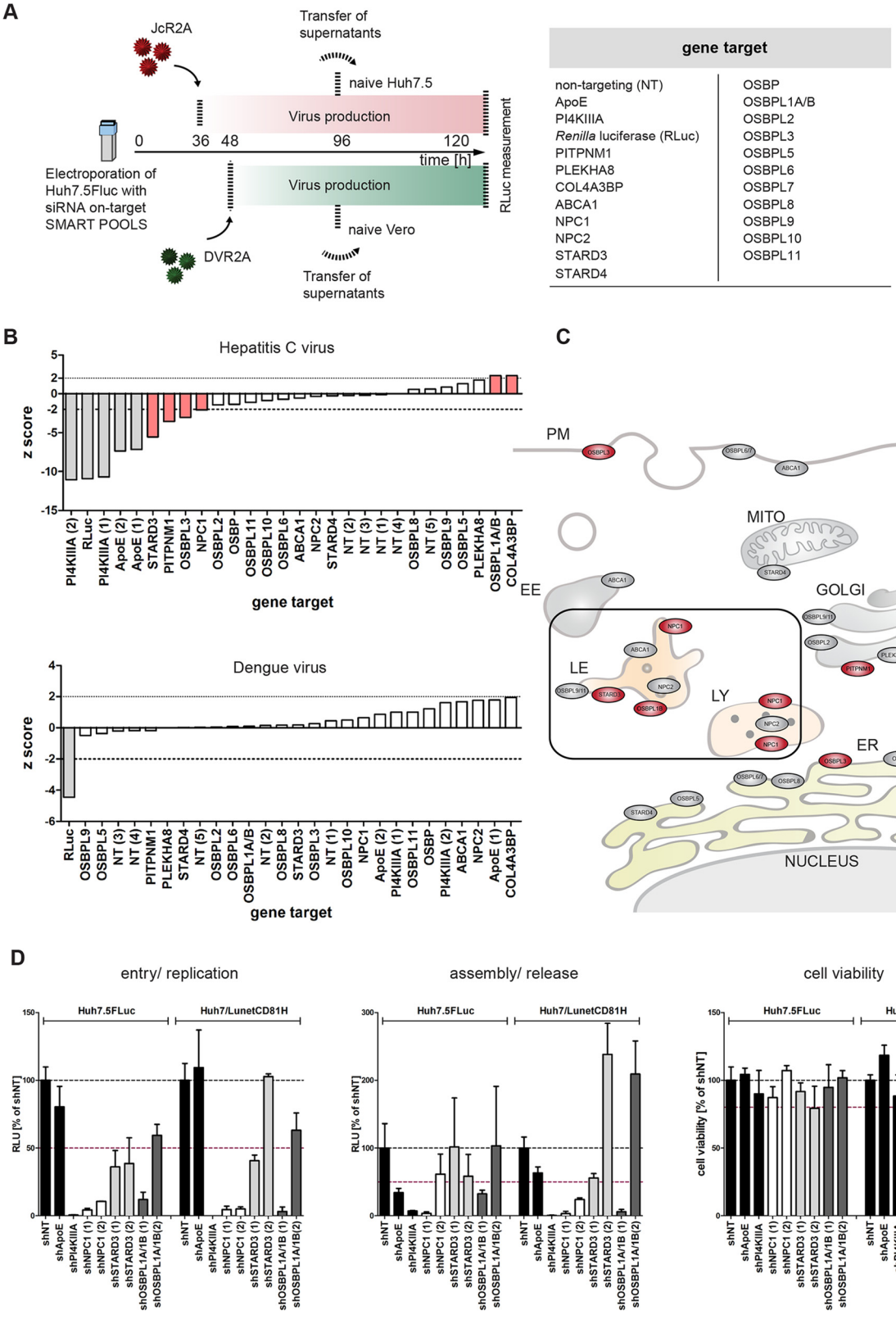

FIG 1 A lipid transfer protein (LTP) RNAi screen leads to the identification of novel host cell factors important for the HCV replication cycle. (A) Screen setup. Huh7.5FLuc cells were electroporated with siRNA pools and seeded in triplicate into 96-well plates. Thirty-six or 48 h later, cells were infected with a *Renilla* luciferase-encoding HCV or DENV reporter virus (JcR2A or DVR2A, respectively) at an MOI of 0.5. After 48 h (DENV) or 60 h (HCV), cell culture supernatants were harvested and transferred onto naive Huh7.5 (HCV) or Vero (DENV) cells to measure virus production. For this purpose, cells were harvested 2 days after infection, and *Renilla* luciferase activity was measured. The RNAi screen was repeated 6 times, each time using a different plate layout. The table on the right displays the target genes studied in the RNAi screen. (B) Representation of the

(Continued on next page)

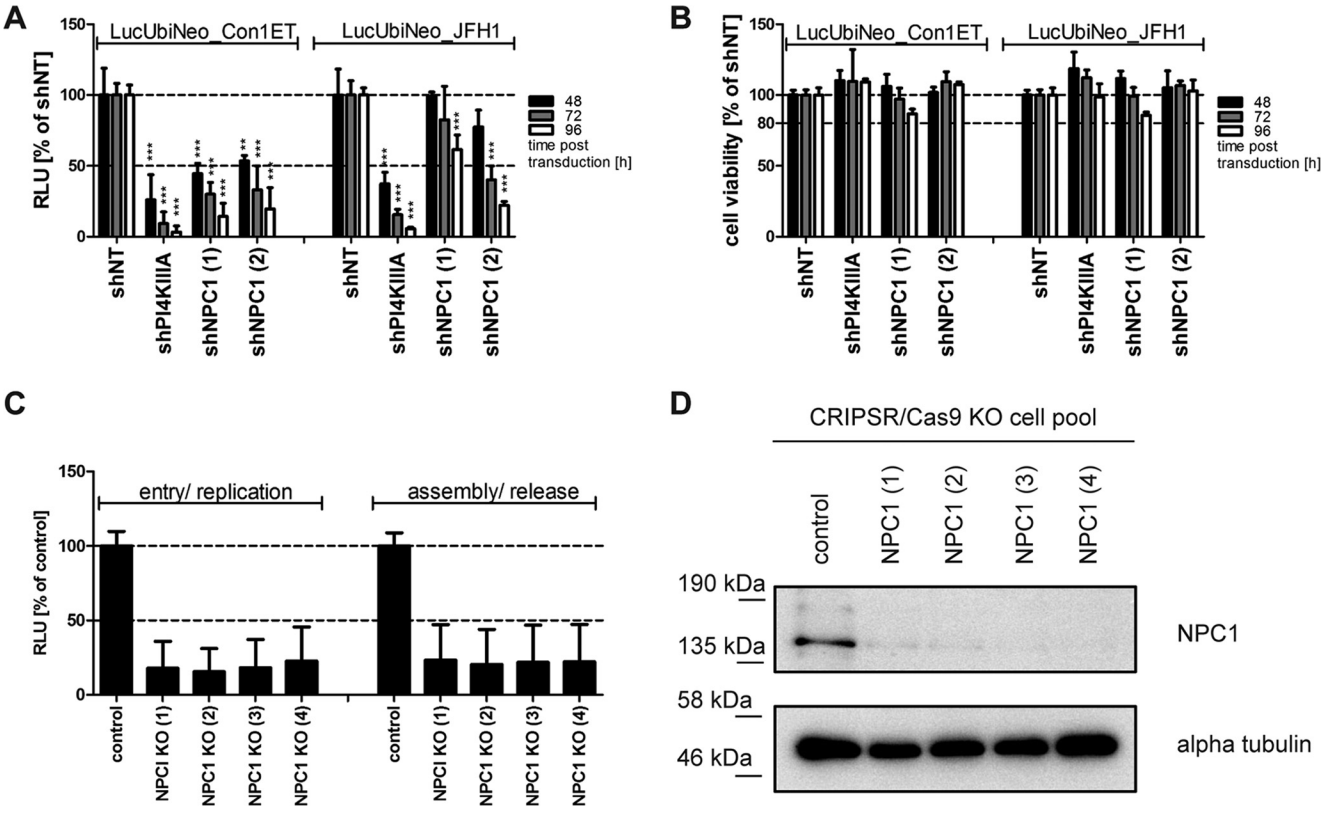

FIG 2 NPC1 is required primarily for HCV RNA replication. (A) Effect of shRNA-mediated knockdown of NPC1 expression on replication of stable subgenomic replicons. Stable firefly luciferase replicon cell lines of genotype 1b (LucUbiNeo_Con1ET) and genotype 2a (LucUbiNeo_JFH1) were transduced with shRNA-encoding lentivirus (MOI = 4). The effect of knockdown on HCV replication was assessed at 48, 72, and 96 h postransduction by measuring firefly luciferase activity in cell lysates. Means and standard deviations for 3 or 4 independent experiments are shown. RLU, relative light units. (B) Cell viability in the experiments summarized for panel A was measured by determining intracellular ATP levels. (C) Huh7-derived cell pools were generated by CRISPR/Cas9 technology, using 4 independent guide RNAs (RNAs 1 to 4). Cells transduced with a nontargeting guide RNA were generated in parallel and used as a control. Cell pools were electroporated with *Renilla* luciferase full-length HCV genomes (JcR2A), and the effects on viral replication and virus production were determined by luciferase assay. The means for two independent experiments are shown. (D) Representative immunoblot showing the protein levels of NPC1 or alpha tubulin (loading control) in either control cells or the four different NPC1 knockout cell pools. ***, $P < 0.001$; **, $P < 0.01$, *, $P < 0.05$.

end, we generated 4 Huh7-derived cell pools, each obtained with a different guide RNA and resulting in a massive reduction of NPC1 protein abundance (Fig. 2D). Consistent with the knockdown data, HCV replication was profoundly reduced in each of the different cell pools (Fig. 2C). This was not due to an impact on virus entry, because we used electroporation of JFH-1 genomes to bypass the entry step. Moreover, virus production was reduced to the same extent as RNA replication, corroborating our conclusion that NPC1 plays a predominant role in HCV replication but not in virus production.

In the second approach, we assessed the antiviral effect of the cationic amphiphile (CA) U18666A, recently described to directly target NPC1 function (30) and to interfere

FIG 1 Legend (Continued)
screen results for HCV and DENV (upper and lower panels, respectively). For each gene, the Z-score is displayed. Controls are indicated in gray, and hits with a Z-score of <-2 or >2 and a *P* value of <0.05 are indicated in red. (C) Subcellular distribution of all candidates analyzed in the screen. Hits are highlighted in red. Note that some proteins are present at several sites within the cell. (D) Effects of shRNA-mediated gene knockdown on entry/replication (left) and assembly/release (middle) of the HCV *Renilla* luciferase reporter virus and on cell viability (right). Cells were transduced with an shRNA-encoding lentivirus and infected with JcR2A 48 h later. Cells were lysed at 48 h postinfection (entry/replication), and cell supernatants were used for infection of naive Huh7.5 cells for 48 h (assembly/release). Means and standard deviations for two independent experiments are shown. RLU, relative light units; ApoE, apolipoprotein E; PI4KIIIA, phosphatidylinositol 4-kinase III alpha; PITPNM1, phosphatidylinositol transfer protein membrane associated 1; PLEKHA8, pleckstrin homology containing A8; COL4A3BP, collagen type IV alpha 3 binding protein; ABCA1, ATP binding cassette subfamily A member 1; NPC1, Niemann-Pick type C1; NPC2, Niemann-Pick type C2; STARD, steroidogenic acute regulatory protein-related lipid transfer domain; OSBP, oxysterol-binding protein; OSBPL, oxysterol-binding protein-related protein.

with endosomal cholesterol transport. We furthermore included the cationic amphiphile Ro 48-8071, which has been suggested to exert a similar inhibition of cholesterol transport (31). In the initial set of experiments, we studied the impacts of the drugs on viral genome amplification and virus production (Fig. 3A, upper left panel). To omit drug effects on viral entry, *in vitro* transcripts of the HCV reporter genome JcR2A were electroporated into Huh7/Lunet cells. As these cells express only low levels of CD81 (32), viral spread is largely restricted, which allowed us to assess drug effects predominantly on genome replication. Short-term treatment for 24 h caused a predominant reduction in virus production, with only minor effects on RNA replication (Fig. 3A, upper right panel). This was not due to an impact of the drug on the infectivity of released virus or on viral entry in the virus titration assay, because cells were extensively washed 4 h prior to supernatant harvest. Therefore, only drug-free supernatants were used for virus titer measurements. Interestingly, upon long-term drug treatment for up to 96 h, we observed an approximately 2-fold reduction in viral genome replication, with little, if any, additional impact on virus production (Fig. 3A, lower panels). As observed with NPC1 knockdown, cationic amphiphile treatment significantly reduced the replication of stable subgenomic replicons of genotype 1b, whereas RNA replication of the genotype 2a replicon was only moderately affected (Fig. 3B and C).

To assess the impact of the cationic amphiphiles on *de novo* HCV RNA replication and to evaluate genotype dependency, replicon RNAs were transfected into Huh7/Lunet cells that had been treated for 48 h with U18666A or Ro 48-8071 4 h after electroporation (Fig. 3D and E). Under these conditions, RNA replication of several genotypes (1a, 1b, 2a, and 3a) was significantly impaired, with the strongest impact being found for the genotype 1b isolate Con1ET. This result suggests that NPC1 function might be critical for the early steps of viral RNA replication.

HCV reshapes the distribution of unesterified cholesterol. Given the role of NPC1 in the export of unesterified cholesterol from LE/LY compartments (22), we next asked whether HCV RNA replication depends on NPC1-mediated cholesterol transport, e.g., to establish the viral RO. Therefore, we first studied the distribution of unesterified cholesterol upon HCV infection and its dependency on NPC1 function. Since the cholesterol-enriched ROs (7) are derived from ER membranes (6), which generally have a low cholesterol content (12), we wondered whether HCV specifically recruits unesterified cholesterol from sites of high cholesterol content, such as the PM (12). To this end, we analyzed the subcellular distribution of cholesterol by using filipin III, which specifically binds to unesterified cholesterol and forms a fluorescent complex (33). Indeed, we observed a time-dependent redistribution of unesterified cholesterol in HCV-infected cells (Fig. 4A). Early in infection, the distribution resembled that for uninfected cells, characterized by the presence of free cholesterol mainly at the PM or in distinct vesicular structures (Fig. 4A and B). At 48 h postinfection, these vesicular structures appeared to fuse to large web-like clusters in the perinuclear region, where cholesterol partially colocalized with NS5A, a component of the HCV replicase complex (Fig. 4A to C). The accumulation of unesterified cholesterol at the perinuclear region was even more pronounced at 72 h postinfection and differed strikingly from the pattern found for uninfected cells (Fig. 4A, B, and D). This result suggests that HCV might recruit cholesterol, possibly from the PM, to the sites of viral replication.

We next analyzed the fate of fluorescently tagged cholesterol exogenously added to HCV-replicating cells. Topfluor-cholesterol (TFC) has been described to integrate into the PM, followed by its rapid uptake into vesicular structures, trafficking to ER/Golgi membranes, and subsequent esterification and transport to lipid droplets (LDs), thereby mimicking the behavior of cellular cholesterol (34). As observed for endogenous unesterified cholesterol, TFC accumulated in large clusters at the perinuclear region of cells containing replicating HCV (Fig. 5A and B). Furthermore, we observed a time-dependent increase of NS5A-TFC colocalization that was independent of the time point after electroporation when TFC was added (Fig. 5C and D; see Movies S1 and S2 in the supplemental material). This result was not flawed by the nonspecific red fluorescence

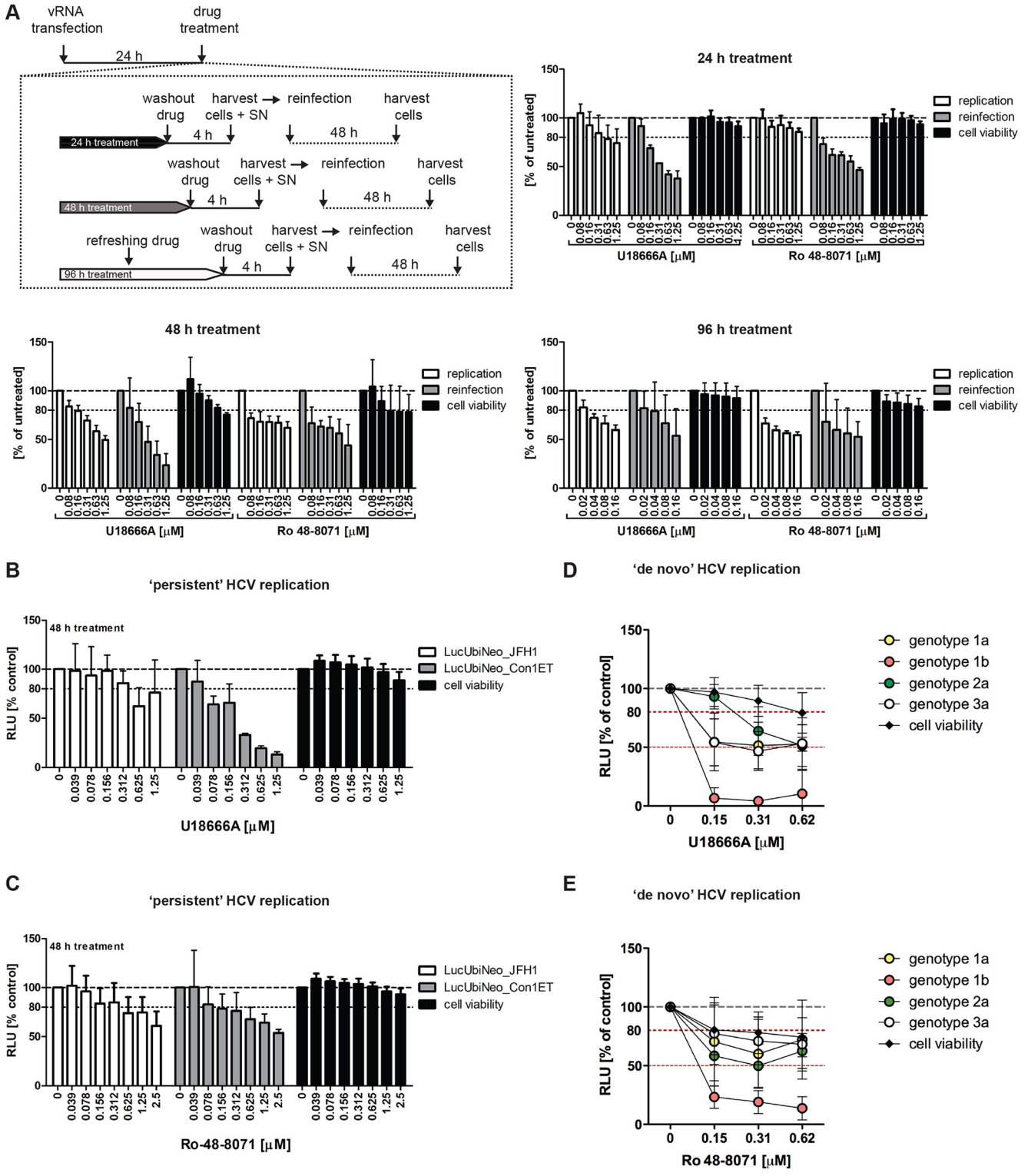

FIG 3 Pharmacological inhibition of NPC1 and its effects on HCV RNA replication and virus production. (A) The experimental setup is shown in the upper left panel. Huh7/Lunet cells were electroporated with the *Renilla* luciferase (RLuc) reporter virus JcR2A and 24 h later treated with U18666A, Ro 48-8071, or water (as a control), using the concentrations specified at the bottom of the bar graphs, for 24, 48, or 96 h. Cells were harvested for luciferase assay, whereas supernatants (SN) were transferred onto naive Huh7.5 cells that were harvested 48 h later for luciferase assay, thus allowing determinations of viral replication and virus production, respectively. The impact of drug treatment on cell viability was assessed by quantifying the intracellular ATP content. Means and standard deviations for 3 or 4 independent experiments are shown. (B and C) Effect of U18666A or Ro-48 8071 treatment on persistent HCV replication. Huh7 cells containing a stable luciferase-encoding subgenomic replicon of genotype 2a (LucUbiNeo_JFH1) or genotype 1b (LucUbiNeo_Con1ET) were treated for 48 h with the given drug concentrations. RNA replication was assessed by measuring firefly luciferase activity in cell lysates. Means and standard deviations for 4 or 5 experiments are depicted. (D and E) Genotype-dependent effect of U18666A or Ro 48-8071 treatment on *de novo* HCV RNA replication. Huh7/Lunet cells

(Continued on next page)

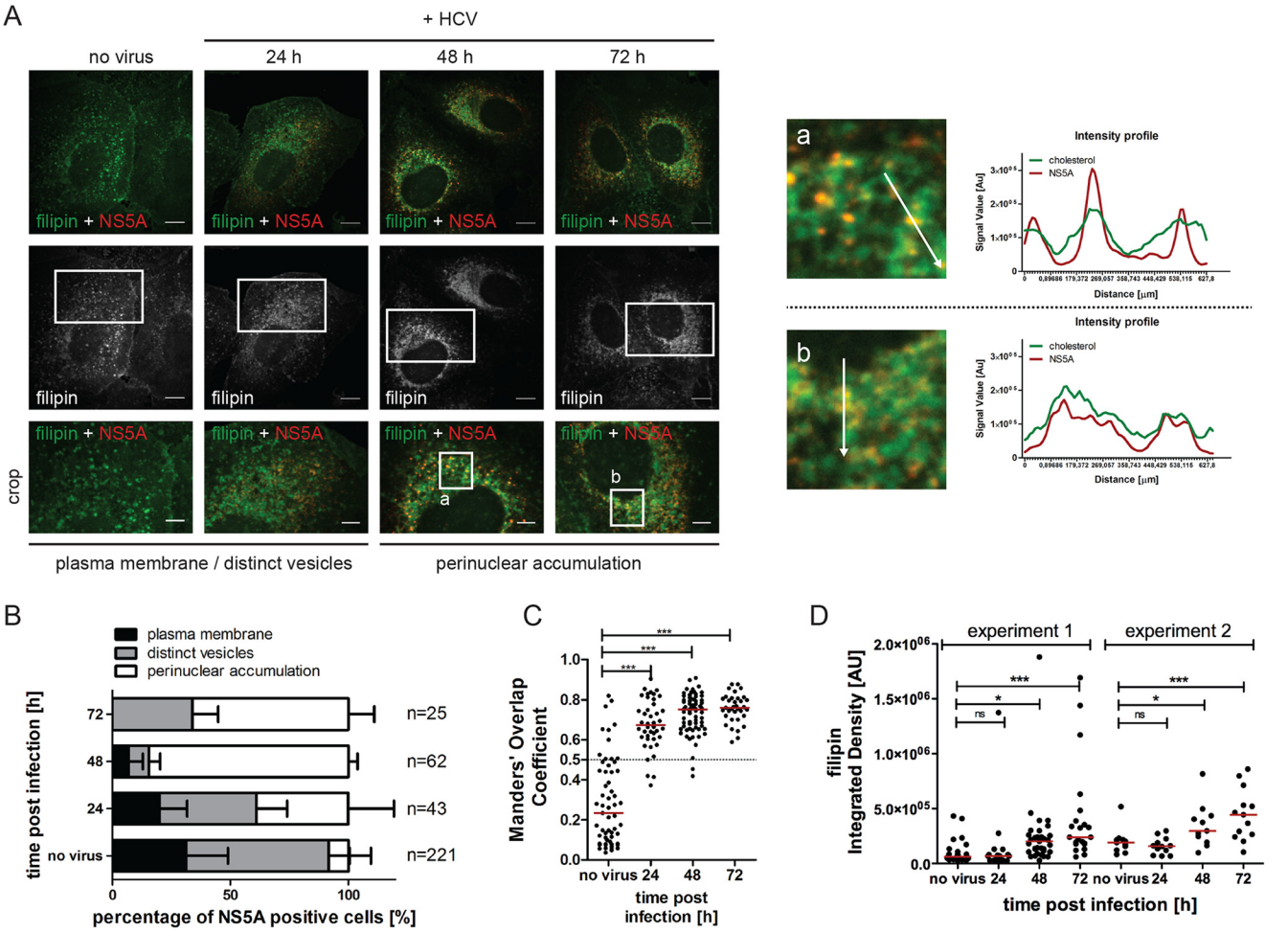

FIG 4 Accumulation of unesterified cholesterol in HCV-infected cells and colocalization with NS5A. (A) Time-dependent subcellular distribution of unesterified cholesterol in HCV-infected cells. LunetCD81H cells were infected with the HCV full-length genome Jc1 (MOI = 3) and fixed at 24, 48, and 72 h postinfection. NS5A (red) was visualized by indirect immunolabeling. Unesterified cholesterol (gray) was labeled using the fluorescence-free cholesterol marker filipin (33). Representative images for each time point after infection are depicted. The areas highlighted with white rectangles in the middle panels are shown in the cropped images below. Therein two areas (a and b) are highlighted, which are shown as enlargements in the right panel. The adjacent histograms indicate the signal intensity profiles of NS5A and cholesterol along the respective arrow. Bars, 10 μm. (B) Quantification of time-dependent changes of cholesterol distribution patterns, classified into the following groups: (i) cholesterol mainly present at the plasma membrane, (ii) cholesterol mainly distributed in a vesicular pattern, and (iii) cholesterol accumulating in a web-like diffuse perinuclear structure. Results for at least two independent experiments are shown (*n*, total number of cells per condition). (C) Quantification of the degrees of colocalization (Manders overlap coefficients) of NS5A and filipin at 24, 48, and 96 h postinfection. Results for two independent experiments are shown; the total number of cells per condition was ≥36. (D) Quantification of the filipin signals at 24, 48, and 72 h postinfection. The integrated fluorescence densities of the filipin signals in NS5A-positive or -negative (no virus) cells were quantified and are given in arbitrary units (AU). Results of two representative experiments are shown. The number of cells per condition was ≥11. ***, $P < 0.001$; **, $P < 0.01$, *, $P < 0.05$; ns, not significant.

signal that can arise from TFC accumulating in small dotted structures, as no colocalization was detected in mock-electroporated cells and TFC-treated cells (Fig. 5E and F).

Although TFC colocalized to NS5A-positive structures that appeared to be lipid droplets as deduced from costaining with the neutral lipid stain LipidTOX Deep Red, a large fraction of TFC and NS5A double-positive structures did not stain with this neutral lipid dye (Fig. 6A). Therefore, we determined the subcellular compartment where NS5A and TFC colocalized by using correlative light electron microscopy (CLEM) (Fig. 6B). To this end, we transfected Huh7/Lunet cells with a subgenomic replicon encoding a fully

FIG 3 Legend (Continued)
were transfected with subgenomic firefly luciferase reporter replicons of genotypes 1a, 1b, 2a, and 3a, and 4 h later, drugs were added to the medium at the concentrations specified at the bottom of the graphs. HCV replication was determined by luciferase assay 48 h after transfection. Cell viability in the same lysate was assessed as described above. Means and standard deviations for 4 independent experiments are shown. RLU, relative light units.

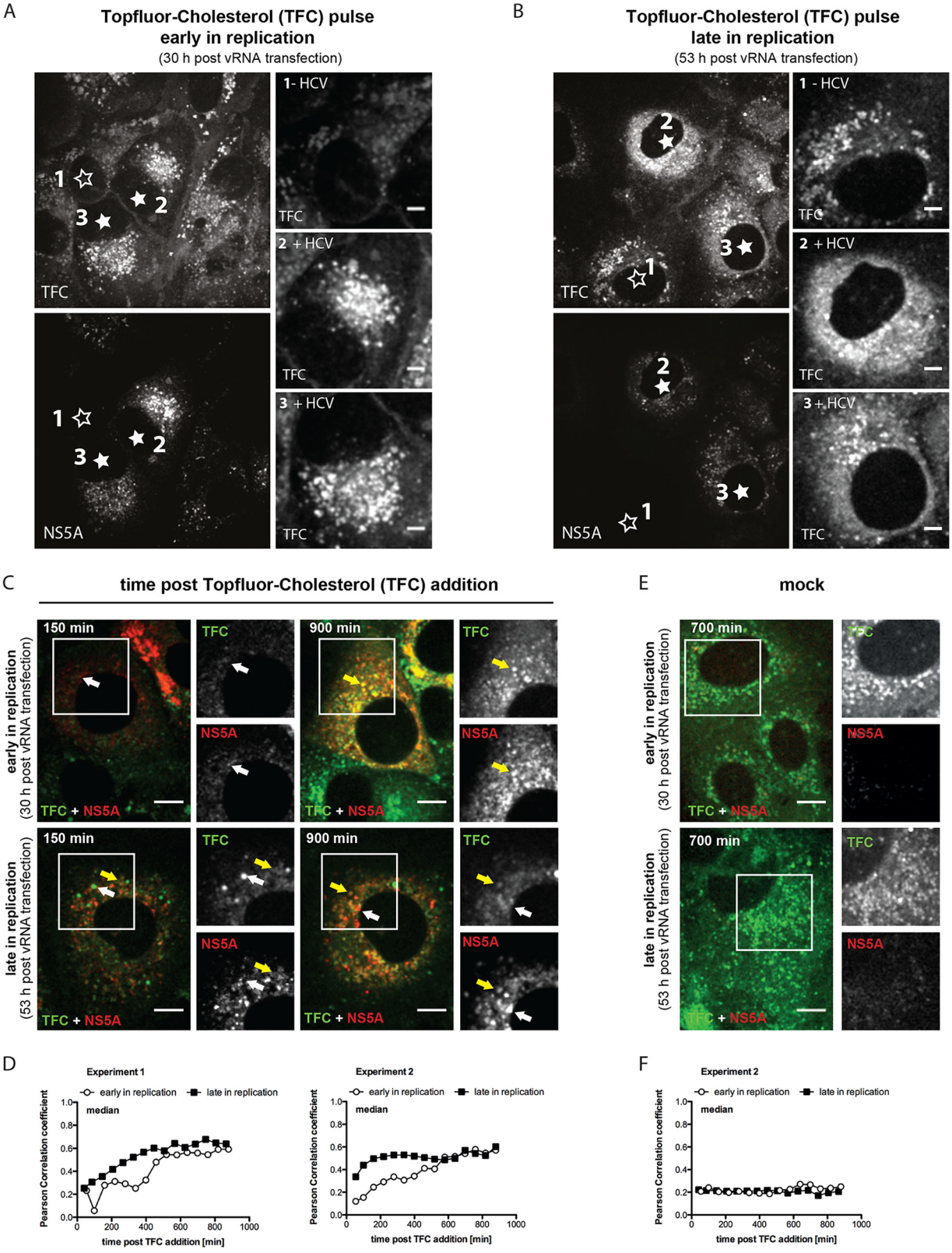

FIG 5 Distribution of exogenously added cholesterol in HCV-replicating cells as determined by live-cell imaging. Huh7/LunetCD81H cells expressing the HCV proteins core to NS2 (LunetCD81H_core-NS2) were transfected with a subgenomic replicon encoding a fully functional mCherry-tagged NS5A protein to allow the production of infectious HCV-like particles (79). Topfluor-cholesterol (TFC; 1 μM) was added 30 h (A) or 53 h (B) after transfection, and the distribution of TFC and NS5A was monitored by live-cell imaging. Images were taken at 900 min post-TFC addition. Untransfected cells (− HCV; empty stars) served as a reference for comparison with cells containing a replicon (+ HCV; filled stars). Enlargements of the cells indicated by white numbers are presented in the adjacent right panels. Bars, 5 μm. (C) Kinetics of intracellular trafficking

(Continued on next page)

functional mCherry-tagged NS5A protein (35) and treated cells with TFC 24 h after transfection. For each fluorescent signal identified by confocal microscopy, the area was measured and correlated with the EM image. In this way, we identified the following ultrastructures (Fig. 6B and C): DMVs remote from LDs (panels a), DMVs at LDs (panels b), LE/LY (panels c), no discernible structure (panels d), and LDs (panels e). These results suggest that a fraction of NS5A and TFC colocalize at DMVs and that exogenously added TFC becomes incorporated into the viral RO as well as into lipid droplets and other, not clearly defined sites (Fig. 6D and E). Nevertheless, we note that the degree of correlation differed between individual cells (Fig. 6B and C). For instance, while in one cell most of the NS5A signal (74% of NS5A and 27% of TFC) could be assigned to DMVs and LDs, which are both known sites of NS5A localization (7, 36), in another cell smaller percentages of NS5A and TFC (ca. 29% and 21%, respectively) localized to these structures and with each other (Fig. 6D and E). Despite this cell-to-cell variability, our data provide evidence that exogenously added TFC is transported to DMVs, where NS5A also accumulates.

NPC1 inhibition causes intracellular accumulation of free cholesterol in lysosomal organelles and disrupts cholesterol colocalization with NS5A. Loss of NPC1 function in neuronal cells is the cause of a lethal lysosomal storage disorder characterized by the intracellular accumulation of unesterified cholesterol (37). Therefore, we investigated the impact of loss of NPC1 function on the distribution of unesterified cholesterol in HCV-replicating cells (Fig. 7). By using NPC1 knockdown, we found that cholesterol accumulated in enlarged clusters intracellularly, whereas in control cells transduced with the nontargeting shRNA the lipid was present at the PM and more evenly distributed in the cytoplasm (Fig. 7A and C). In the case of the PI4KIIIA knockdown that served as a control, cholesterol appeared to be more dispersed throughout the cell (Fig. 7A). When we assessed the impact of U18666A or Ro 48-8071 on the distribution of unesterified cholesterol, treatment with U18666A caused an accumulation of unesterified cholesterol in lysosomal structures that were significantly enlarged compared to those in control cells, thus resembling the NPC1 knockdown phenotype (Fig. 7B and C), and a similar result was obtained upon treatment with Ro 48-8071 (Fig. 7B and C).

Given that upon treatment with either drug, unesterified cholesterol accumulated in LAMP1-positive structures (Fig. 8A), and since both drugs are suggested to additionally target enzymes of the cholesterol biosynthesis pathway (38, 39), we asked whether drug treatment caused an altered lipid distribution or affected overall cholesterol content. By quantifying the filipin signal obtained with drug-treated or control cells, we observed comparable cholesterol contents, suggesting that these drugs affected predominantly cholesterol distribution under the conditions used here (Fig. 8B). In addition to an altered subcellular lipid distribution, the localization of NS5A changed upon drug treatment, with NS5A forming aggregates and becoming excluded from filipin-positive structures (Fig. 8A, white arrows). These results argue for a defect of the export (and possibly degradation) of PM-derived cholesterol from lysosomal organelles upon cationic amphiphile treatment or NPC1 knockdown. As a consequence, unesterified cholesterol would not be transported to the viral replication sites. In line with this assumption, colocalization of NS5A and filipin was reduced in cells treated with U18666A or Ro 48-8071 (Fig. 8C). Importantly, at the concentrations tested, NS5A

FIG 5 Legend (Continued)
of TFC and NS5A-mCherry in replicon-transfected cells. The localization of NS5A and TFC, added 30 h (upper panels) or 53 h (lower panels) post-HCV RNA transfection, was imaged in live LunetCD81H_core-NS2 cells for the given time spans. Representative images for two different time points are shown. White rectangles mark the areas for which NS5A or TFC insets are depicted on the right. White arrows point to either TFC or NS5A structures that do not overlap, whereas yellow arrows indicate structures that are TFC and NS5A positive. Bars, 10 μm. The intensity of the signals was adjusted to facilitate visualization. (D) Quantification of the degree of NS5A and TFC signal overlap throughout the observation period as determined by use of the Pearson correlation coefficient. The medians for two independent experiments are shown; 4 or 5 cells were analyzed per experiment and per condition. (E) Representative images of mock-transfected cells to which TFC was added at 30 or 53 h postelectroporation. (F) Quantification of the degree of NS5A and TFC signal overlap throughout the observation period as determined by use of the Pearson correlation coefficient. The medians for 4 or 5 cells per condition are shown.

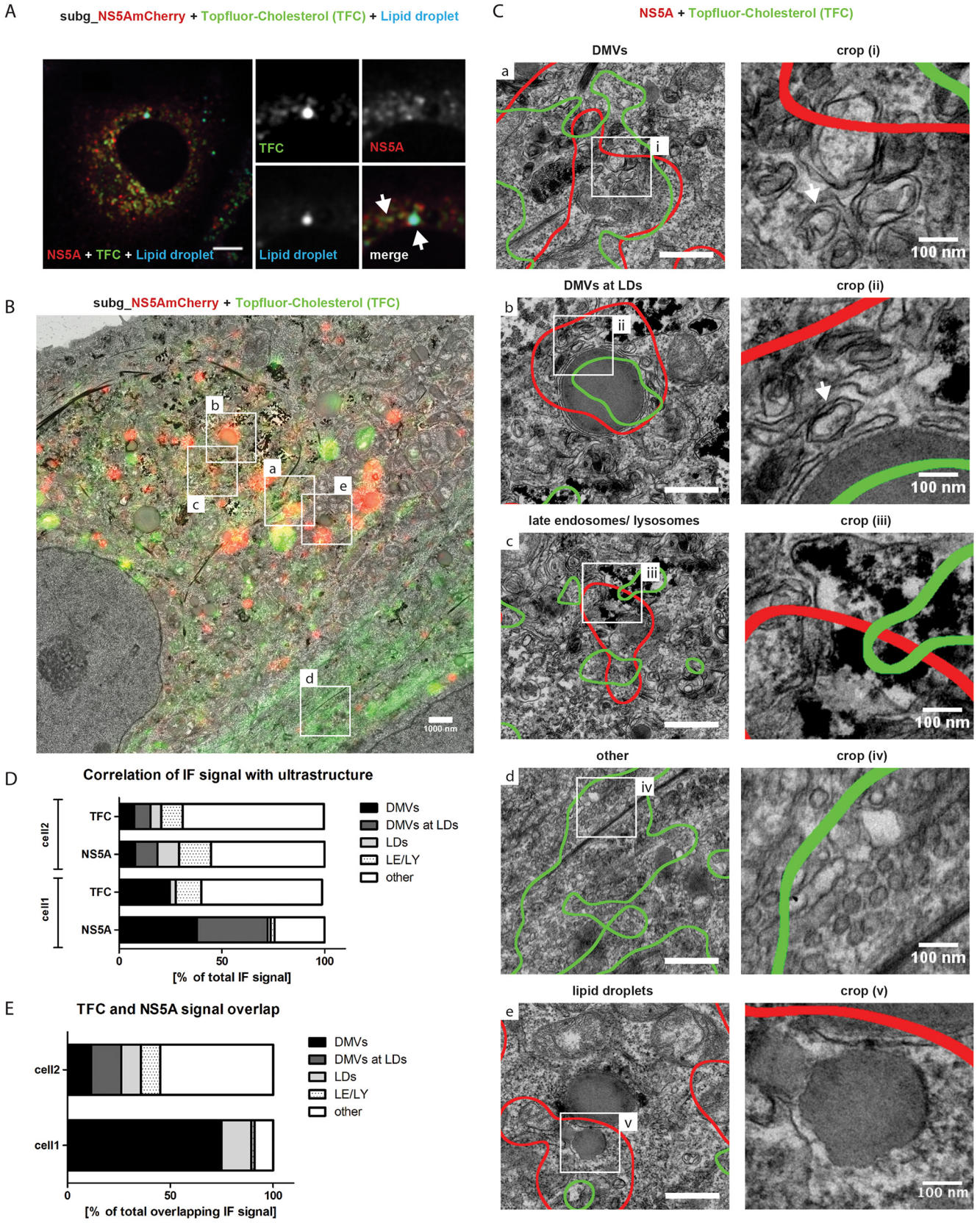

FIG 6 Analysis of the ultrastructure of NS5A- and Topfluor-cholesterol (TFC)-positive cells by correlative light electron microscopy on HCV-replicating cells. (A) Huh7/LunetCD81H cells expressing the HCV proteins core to NS2 were transfected with a subgenomic replicon (isolate JFH-1) encoding a fully functional mCherry-tagged NS5A protein. Topfluor-cholesterol (TFC; 1 μM) was added 53 h after HCV RNA transfection, and 16 h later, LipidTOX Deep Red neutral stain

(Continued on next page)

abundances were comparable between mock and drug-treated cells as determined by fluorescence microscopy and immunoblotting (Fig. 8D and E, respectively). Therefore, we concluded that interfering with NPC1-mediated cholesterol transport causes the accumulation of unesterified cholesterol in lysosomal vesicles and likely interferes with cholesterol transport to the viral RO.

To further support our hypothesis that the uptake of exogenous cholesterol is important for viral RNA replication, we assessed the impact of depletion and replenishment of exogenous lipids on HCV replication. We cultured Huh7-derived cell lines containing stable replicons of genotype 1b or 2a in complete medium or medium lacking lipids (lipid-free Dulbecco's modified Eagle's medium [LF-DMEM]) or in the same medium supplemented with human LDL (Fig. 9A). We found that replication of the genotype 1b replicon (isolate Con1) was reduced upon lipid withdrawal but restored to normal levels upon addition of exogenous LDL, while there was no effect on cell viability (Fig. 9B and C). This result supported the notion that exogenous lipids are important for efficient HCV RNA replication, though only a minimal effect was found with the HCV isolate JFH-1, arguing for genotype- or replication capacity-specific differences.

NPC1 function is important for integrity of the membranous web. Recent publications indicated that HCV usurps host cell factors, such as OSBP, in order to recruit cholesterol to the RO, where it might contribute to the morphology of the DMVs (14). However, the origin of the transported cholesterol is unknown. We found that exogenous lipids are important for viral RNA replication (Fig. 9) and that impairment of NPC1 function causes an accumulation of unesterified cholesterol in lysosomal organelles (Fig. 7 and 8), thus restricting cholesterol accessibility by cytosolic acceptors, such as members of the OSBPL family. To investigate whether NPC1 and OSBP possibly act in concert, we assessed the impact of pharmacological inhibition of both of these factors on viral RNA replication (Fig. 10A and B). To this end, we first treated stable replicon cell lines of genotypes 1b and 2a (LucUbiNeo_Con1ET and LucUbiNeo_JFH1, respectively) with 0.625 μM U18666A or Ro 48-8071 (water treatment served as a control). After 24 h, the supernatant was replaced with medium containing the same drug again as well as 1 nM OSW-1, a commonly used OSBP inhibitor (14), or dimethyl sulfoxide (DMSO) (as a control) for another 24 h. The combination of both drugs had a stronger impact on viral replication than treatment with either drug separately (Fig. 10A), although some effect due to reduced cell vitality cannot be excluded (Fig. 10B).

Since these results indicated that OSBP and NPC1 might act in a concerted manner, we argued that interference with endosomal cholesterol transport should affect the integrity of the membranous web, as cholesterol is an important component of DMVs (7, 14). For this reason, we investigated the ultrastructure of the membranous web in cells transfected with a subgenomic replicon and treated with a cationic amphiphile. In untreated cells transfected with a subgenomic replicon, single-, double- and multimembrane vesicles were observed, which were not detected in naive Huh7 cells (Fig. 10C). DMVs had a median diameter of 186 nm (Fig. 10D and E). Upon treatment with two different concentrations of U18666A shown to cause a drop in cholesterol/NS5A colocalization (Fig. 8C), we observed a dose-dependent decrease of the DMV diameter (Fig. 10D and E). Likewise, treatment with 1.25 μM Ro 48-8071 significantly reduced the

FIG 6 Legend (Continued)
to label lipid droplets was added. After 20 min, cells were imaged. A representative image is displayed, showing the distribution of TFC (green), NS5A (red), and lipid droplets (blue). The white arrows indicate areas where either all three signals or only NS5A and TFC overlap. Bar, 10 μm. (B) Huh7/Lunet cells were transfected as described for panel A and after 32 h pulsed with 1 μM TFC and incubated for another 12 h. Cells were fixed and processed for light microscopy and subsequent electron microscopy. The large panel shows an overview of the correlation of the NS5A (red) and TFC (green) signals. The white boxes indicate selected areas displayed in panel C. Each region of interest (ROI) was classified as follows: ROIs mostly covering DMVs (a), DMVs at LDs (b), late endosomes/lysosomes (c), other regions of the cells (d), and lipid droplets (e). For each example image, a magnified view is given in the adjacent panel (views i to v). The white arrows indicate DMVs. Bar, 500 nm for the lower-resolution images. (D) Results of correlative analysis of two cells. Areas of TFC and/or NS5A signal as explained for panel B were quantified. (E) Quantification of TFC and NS5A signal overlap in two different cells for the specified subcellular regions.

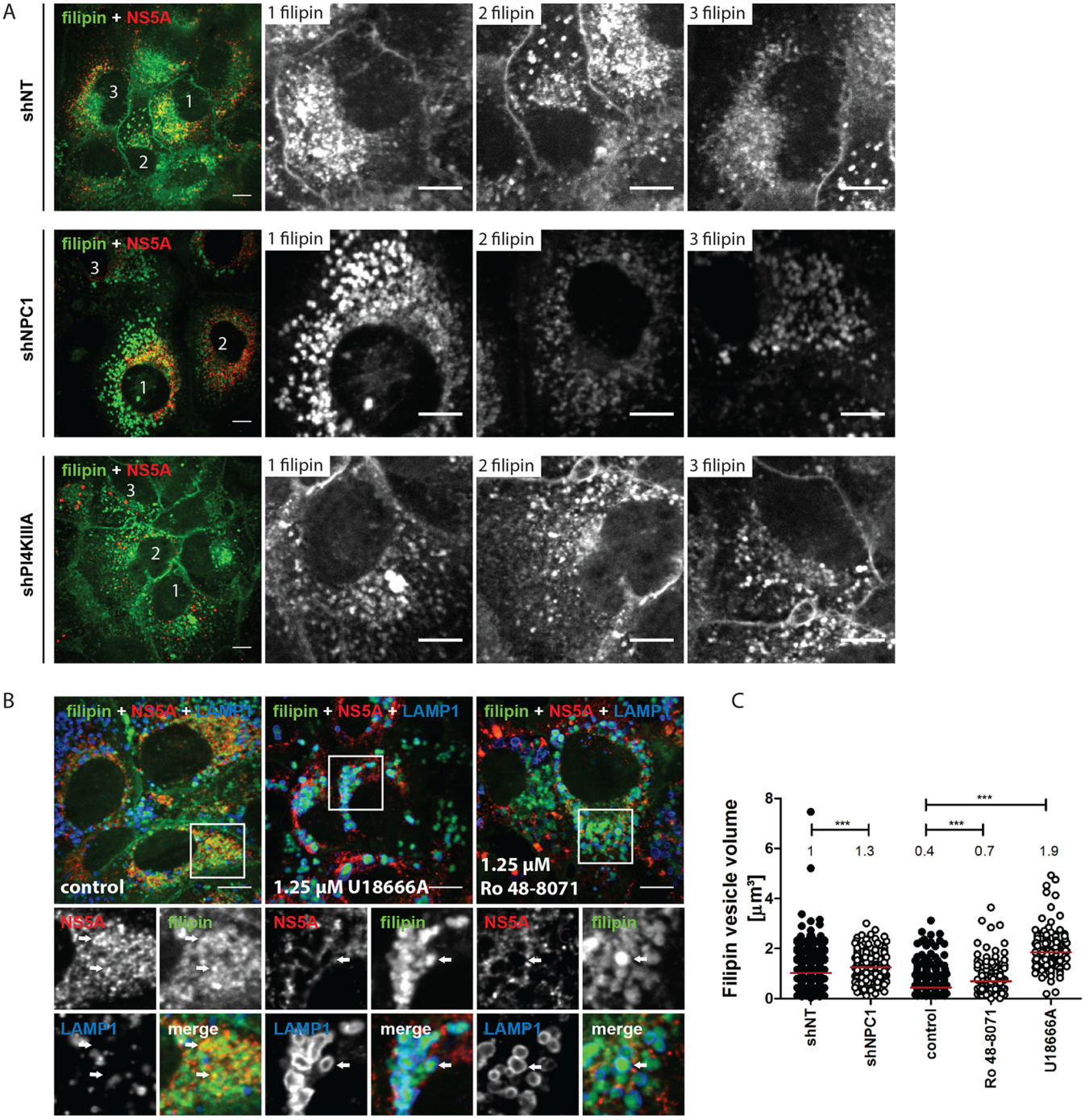

FIG 7 Knockdown of NPC1 or its pharmacological inhibition alters the distribution of endogenous unesterified cholesterol. (A) Huh7/Lunet cells were transfected with the HCV full-length genome Jc1, and 4 h later, cells were transduced with a lentivirus (MOI = 4) encoding NPC1- or PI4KIIIA-specific shRNAs or a nontargeting shRNA (shNT) serving as a control. Sixty-eight hours later, cells were fixed, and free cholesterol (filipin; green) and NS5A (red) were visualized by indirect immunolabeling. The left panels show merged images, while the adjacent images display the filipin signal for each of three different cells. (B) Huh7/Lunet cells were transfected with the HCV full-length genome Jc1, and 24 h later, cells were treated with U18666A or Ro 48-8061 for 48 h. Free cholesterol (filipin; green), NS5A (red), and the lysosomal marker LAMP1 (blue) are shown. White arrows indicate NS5A either colocalizing with filipin (control) or not (drug-treated cells). (C) Quantification of the volumes of filipin-positive structures in the cells shown in panels A and B. At least 200 structures in 10 to 13 cells were analyzed. The red bars and numbers indicate the medians. ***, $P < 0.001$; **, $P < 0.01$, *, $P < 0.05$. Bars, 10 μm.

median DMV diameter (Fig. 10C to E). Importantly, the changes in DMV morphology were not caused by altered viral protein abundance as determined by NS5A-specific immunoblotting (Fig. 10F). Whether this unaltered NS5A level reflects decreased protein turnover in drug-treated cells is not known.

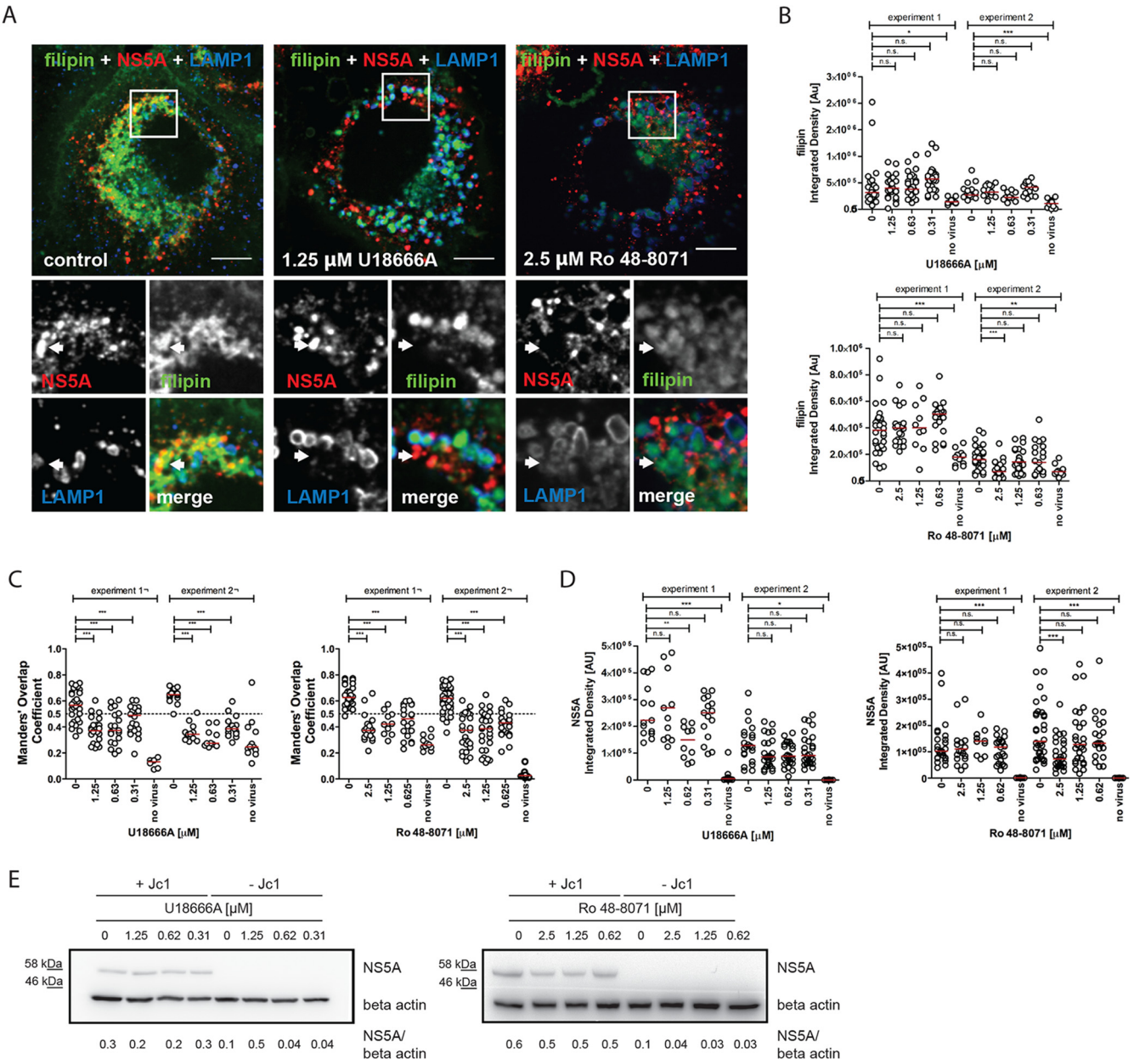

FIG 8 Analysis of cholesterol and NS5A abundances and their colocalization upon U18666A or Ro 48-8071 treatment. (A) Huh7/Lunet cells were transfected with the HCV full-length genome Jc1. After 24 h, cells were treated with the given drug concentrations for 48 h, and after fixation, free cholesterol (filipin; green), NS5A (red), and the lysosomal marker LAMP1 (blue) were visualized. White arrows indicate NS5A either colocalizing with filipin (control cells) or not (drug-treated cells). Representative images of cells treated with either 1.25 μM U18666A, 2.5 μM Ro 48-8071, or water (control) are shown. The signal intensity of filipin (integrated density, in arbitrary units [AU]) (B), the NS5A-filipin signal overlap (Manders overlap coefficient) (C), and the NS5A signal intensity (integrated density, in arbitrary units [AU]) (D) were determined for cells from the experiment shown for panel A. Uninfected and untreated cells are indicated by "no virus." Results for two independent experiments for which at least 10 cells were analyzed are shown. Red bars indicate the medians. Each circle represents the result obtained for a single cell. (E) Representative immunoblot showing the protein levels of NS5A and beta actin under the corresponding conditions analyzed for panels A and B. The numbers on the bottom indicate the NS5A/beta actin signal ratio for two or three independent experiments. Note that NS5A abundance was not significantly affected at any drug concentration used. ***, $P < 0.001$; **, $P < 0.01$, *, $P < 0.05$.

To validate these results in the context of a complete HCV genome, the HCV isolate Jc1 was transfected into Huh7/Lunet cells that were treated 4 h after transfection with U18666A for 48 h. As shown in Fig. 11A to C, we were able to confirm an alteration of membranous web integrity as revealed by a reduced DMV diameter in cells treated with U18666A, although this reduction was less pronounced than the results obtained with the subgenomic replicon. Importantly, NS5A protein levels were similar under all conditions tested (Fig. 11D). In addition, treatment of the cells with the cationic

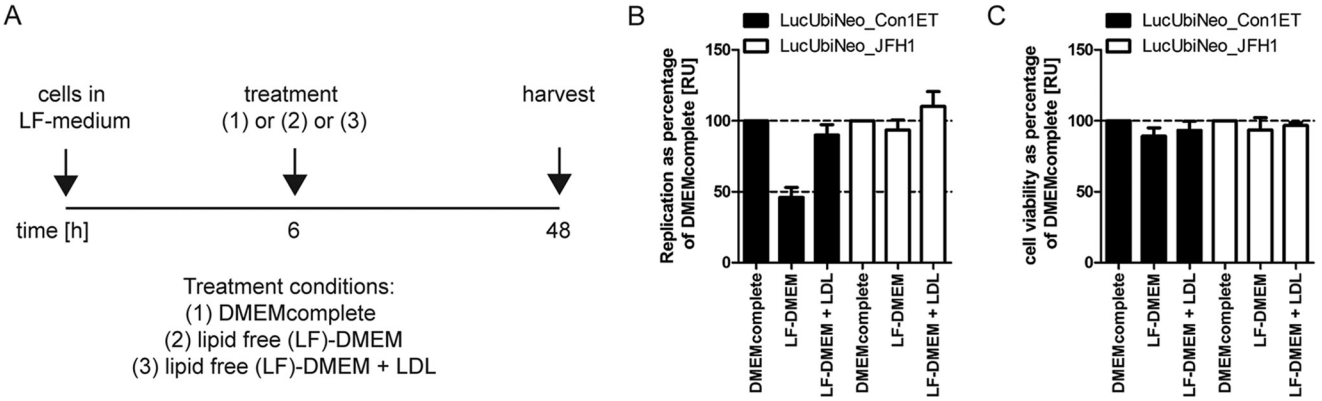

FIG 9 Rescue of HCV replication by LDL in cells cultured under lipid-free conditions. (A) Schematic of the treatment regimen. Huh7-derived cell lines containing stable reporter replicons of genotype 1b (LucUbiNeo_Con1ET) or genotype 2a (LucUbiNeo_JFH1) were cultured in DMEM containing 10% lipid-free fetal calf serum (LF medium). After 6 h, the medium was replaced with either fresh complete DMEM or LF-DMEM supplemented or not with 50 μg/ml human LDL. Cells were harvested 48 h later. (B) HCV RNA replication was determined by firefly luciferase assay and normalized to the values obtained for cells cultured in complete DMEM. (C) Cell viability was assessed by measuring intracellular ATP levels. The results for three independent experiments are shown. RU, relative units.

amphiphile altered the DMV shape, showing protrusions of the innermost membrane toward the DMV lumen (Fig. 11E, black arrows) more often than the case for regular DMV structures (Fig. 11E and F).

In conclusion, these results suggest that HCV exploits NPC1 at ER and LE/LY membrane contact sites to recruit cholesterol to the viral RO, with this lipid contributing to the functionality and integrity of the membranous web.

DISCUSSION

A common feature of positive-strand RNA viruses is the formation of organelle-like membranous compartments serving as sites of viral RNA replication. These ROs can exhibit different morphologies and form either invaginated vesicles or protrusions, such as spherules or DMVs (4). Formation of the ROs most likely involves a concerted action of a multitude of viral and host cell proteins to drive the generation of a microenvironment with a specifically defined protein and lipid composition. Indeed, HCV RNA synthesis was shown to occur at lipid raft-like membrane structures, indicating a unique lipid composition (10, 11). Furthermore, electron microscopy-based analysis of affinity-purified DMVs revealed the enrichment of unesterified cholesterol (7). Considering that DMVs arise from the ER (6), which itself has a low cholesterol content (12), HCV must develop strategies to gather cholesterol and possibly other lipid species and to incorporate them into its ROs. For this reason, we searched for LTPs contributing to HCV replication and RO integrity and identified STARD3, OSBPL1A and -B, and NPC1. The latter was characterized in detail and found to be required for HCV RNA replication. Interestingly, the impact on viral RNA replication was stronger in case of *de novo* RNA replication than in a situation mimicking persistent replication. This may reflect a slow turnover or *de novo* generation of ROs in cases of persistent, i.e., already established, replication, in contrast to a strong dependency on cholesterol access under conditions where ROs have to form during the early stage of replication establishment. Interestingly, upon short-term treatment with an NPC1 inhibitor, the predominant effect was reduced virus production rather than impaired RNA replication. This result is in agreement with an earlier report suggesting an accumulation of infectious HCV particles in lysosomal structures and the inhibition of their release upon short-term U18666A treatment (40). However, upon long-term treatment with the NPC1 inhibitor, the impact on RNA replication predominated, consistent with results obtained by using NPC1 knockout cell pools.

NPC1 is a transmembrane protein present in the limiting membrane of LE/LY (22). Defects in NPC1 function caused by only one of several possible single point mutations

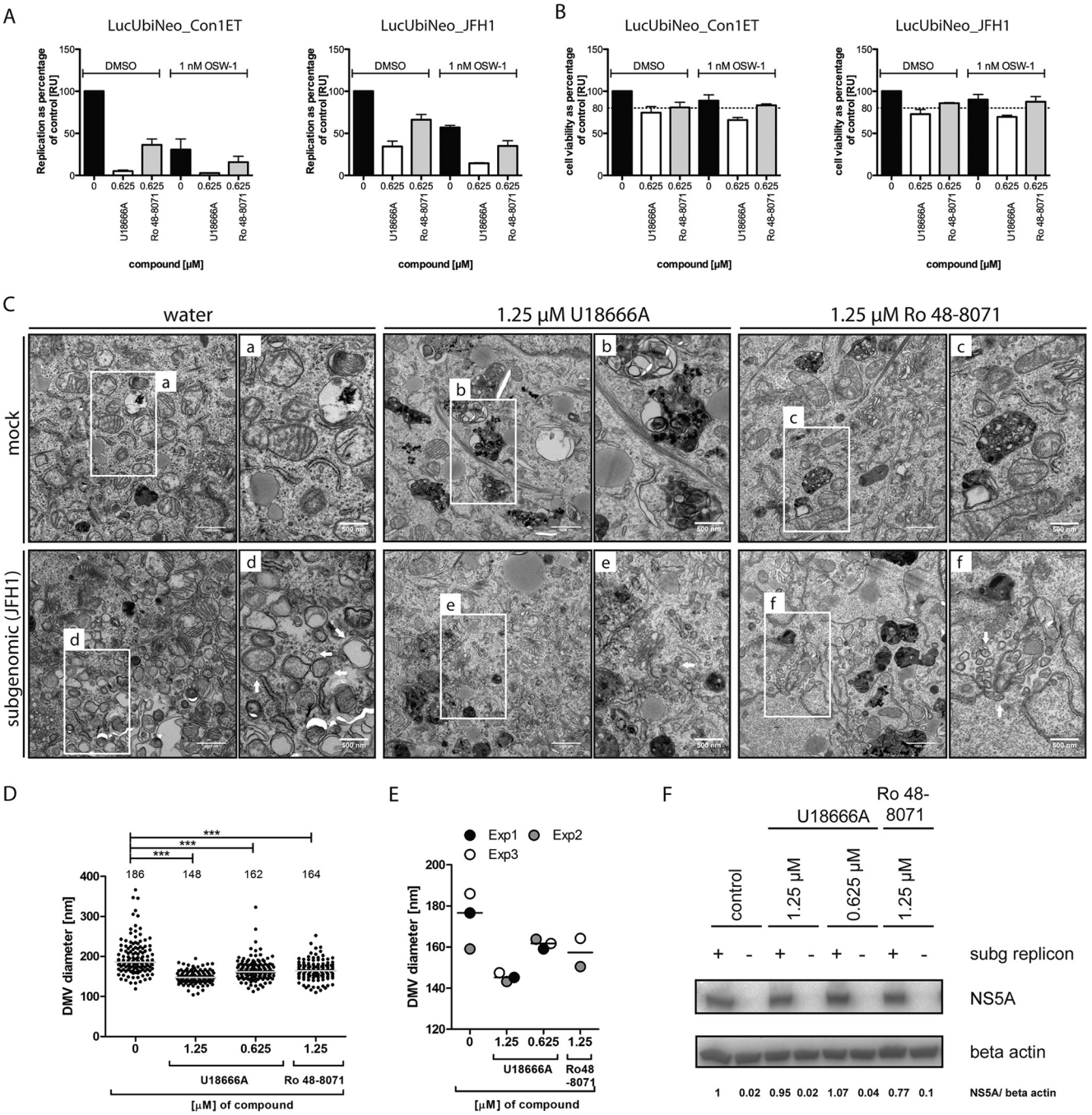

FIG 10 Effect of altered subcellular cholesterol distribution on morphology of the membranous web. (A) The replicon cells specified at the top were treated for 24 h with 0.625 μM U18666A, 0.625 μM Ro 48-8071, or water. Thereafter, the medium was replaced with fresh medium containing either water or the given drug in addition to either DMSO or 1 nM OSW-1. Cells were cultured for an additional 24 h and lysed for measurements of viral RNA replication by firefly luciferase assay (A) and cell viability (B). The results for two independent experiments are shown and are presented as percentages of the untreated control values. (C) Huh7/Lunet cells were electroporated with *in vitro* transcripts of the subgenomic replicon encoding mCherry-tagged NS5A. At 4 h postelectroporation, cells were treated with U18666A or Ro 48-8071 or left untreated, and 42 h later, cells were fixed and processed for electron microscopy analysis. Representative images are shown, with white boxes highlighting the areas shown as enlargements in the adjacent insets. White arrows indicate double-membrane vesicles. (D) DMV diameters were determined for untreated cells or cells treated with 1.25 μM or 0.625 μM U18666A or 1.25 μM Ro 48-8071. The results of a representative experiment are shown. At least 10 cell profiles were analyzed per condition. Each horizontal line indicates the median diameter, which is given numerically above each column. (E) Summary of the results of 2 or 3 independent experiments. The median DMV diameter for each experiment is indicated by a circle, while the black line represents the overall median. (F) Immunoblot showing NS5A abundances in lysates of cells corresponding to panel C; beta actin served as a loading control and for normalization. Numbers below the lanes are the ratios of NS5A and beta actin signals. ***, $P < 0.001$; **, $P < 0.01$, *, $P < 0.05$.

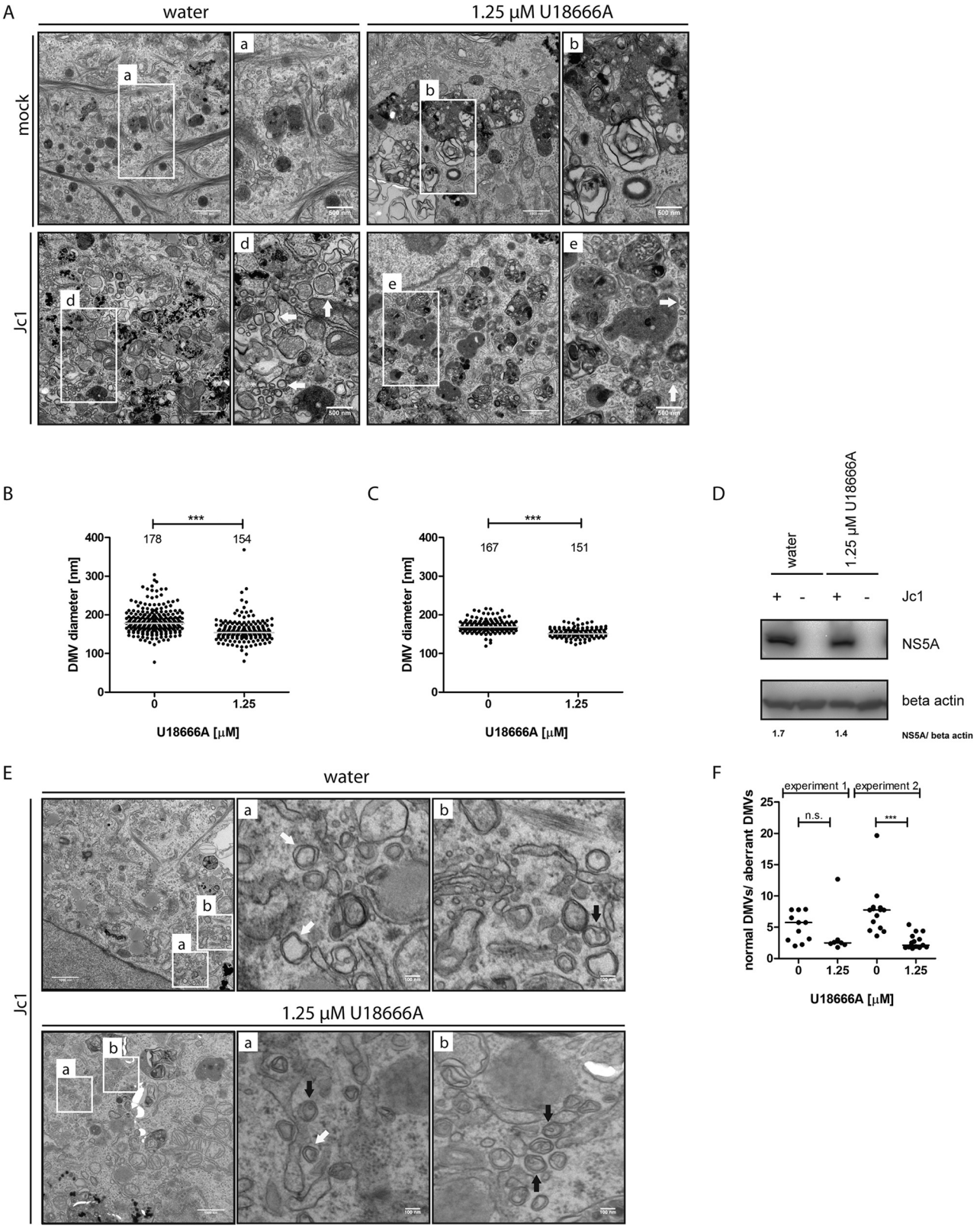

FIG 11 NPC1-mediated cholesterol export at late endosome-lysosome–ER contact sites is important for the integrity of the membranous web in HCV-infected cells. Huh7/Lunet cells were electroporated with full-length RNA of the HCV genome Jc1. At 4 h postelectroporation, cells were treated with 1.25 μM U18666A or left untreated, and 42 h later, cells were fixed and processed for electron microscopy analysis. (A) Representative images, with white boxes highlighting the areas shown in the adjacent insets. White arrows indicate double-membrane vesicles (DMVs). (B and C) DMV diameters were determined for untreated cells or cells treated with 1.25 μM U18666A. Quantifications for two experiments are shown in panels B and C. At least 10 cells were analyzed per condition. Each horizontal line indicates the median, which is given numerically above each column. (D) Representative

(Continued on next page)

(37) have been reported to cause a tremendous intracellular accumulation of unesterified cholesterol in lamellar bodies carrying LE/LY markers (41). Thus, HCV replication may depend on NPC1-mediated cholesterol export from the LE/LY. Indeed, U18666A or Ro 48-8071 treatment mimicked the accumulation of unesterified cholesterol in large lysosomal vesicles observed upon NPC1 knockdown. Importantly, this was concomitant with a decrease of unesterified cholesterol at NS5A-positive sites, arguing for a defect in cholesterol trafficking from the LE/LY compartments to the ROs.

Interestingly, we observed that HCV infection alters the distribution of unesterified cholesterol by inducing its accumulation around the nucleus. In agreement with others (42), we found that exogenously added Topfluor-cholesterol that mimics the partitioning and trafficking of cellular unesterified cholesterol (34) is recruited to NS5A-positive sites. Wang and Tai argued that TFC was mainly recruited to old NS5A sites, representing DMVs and multimembrane vesicles (MMVs), where cholesterol may be important for association of the ROs with LDs, and thus for viral assembly (42). Indeed, we found that NS5A and TFC were present at DMVs in close proximity to LDs, but an even larger fraction of both protein and lipid colocalized to DMVs that were remote from LDs or other cellular organelles. Furthermore, we observed that the depletion of exogenous lipids reduced viral replication, which was rescued upon the addition of exogenous LDL. Taken together, these results suggest that cholesterol, possibly derived from the PM or from the uptake of LDL, is delivered through the endosomal pathway to the viral ROs by the action of LTPs, such as NPC1.

Based on these considerations, we propose that RNA replication depends on endosomal cholesterol homeostasis and cholesterol transport, requiring multiple cellular factors (Fig. 12). One of the key players is cytosolic PI4KIIIA, which becomes recruited and activated by NS5A and NS5B, resulting in a local accumulation of PI4P (16, 17). In addition, HCV coopts the ER-resident VAP proteins A and B (4, 43–45) at DMVs to promote the recruitment of LTPs that possess a VAP binding motif (FFAT motif). One of the key factors for cholesterol transport to DMVs is OSBP most likely delivering cholesterol in exchange for PI4P (14). Yet the source of cholesterol delivered by LTPs, such as OSBP, is unclear. Based on our results, we hypothesize that NPC1 transfers cholesterol from LE/LY compartments to cellular acceptors, such as members of the ORP family (Fig. 12). Indeed, we observed that the inhibition of OSBP in addition to NPC1 had a stronger impact on replication than impairment of only one of the cellular factors, arguing for a concerted action of both. Interestingly, knockdown of another member of the ORP family, the ER resident OSBPL5, was shown to cause the accumulation of unesterified cholesterol in the limiting membrane of LE/LY, while NPC1 knockdown manifests as cholesterol entrapment within the vesicle, arguing that OSBPL5 might act as another cytosolic acceptor of cholesterol downstream of NPC1 (46, 47) (Fig. 12). Furthermore, another VAP binding protein, OSBPL1B (ORP1L), has been reported to regulate the positioning of LE according to their cholesterol content and the establishment of LE-ER contact sites. In uninfected cells, OSBPL1B (ORP1L) tethers endosomes of low cholesterol content to the ER via interaction with VAP proteins and causes a dispersed distribution of these vesicles. At high endosomal cholesterol levels, OSBPL1B promotes the coupling of the vesicles to dynein motor proteins and vesicle transport to the microtubule minus ends (26, 48). Although we do not know whether HCV makes use of OSBPL1B (ORP1L) to recruit cholesterol-loaded endosomal vesicles and to promote the establishment of LE-ER membrane contact sites, the impaired HCV RNA replication observed upon knockdown of OSBPL1B (ORP1L) supports such a model.

By using an RNAi-based approach, we also identified ABCA1 and STARD3 as host cell

FIG 11 Legend (Continued)
immunoblot showing NS5A and beta actin abundances in cell lysates corresponding to panel A. The numbers indicate the NS5A/beta actin signal ratios determined for two independent experiments. (E) Representative images showing DMVs with regular (white arrows) or aberrant (black arrows) morphology. (F) Quantification of the ratio of DMVs with regular morphology to DMVs with an aberrant shape. Each dot indicates the ratio determined for a single cell. The results of two independent experiments are shown. Each horizontal line indicates the median. ***, $P < 0.001$; **, $P < 0.01$, *, $P < 0.05$.

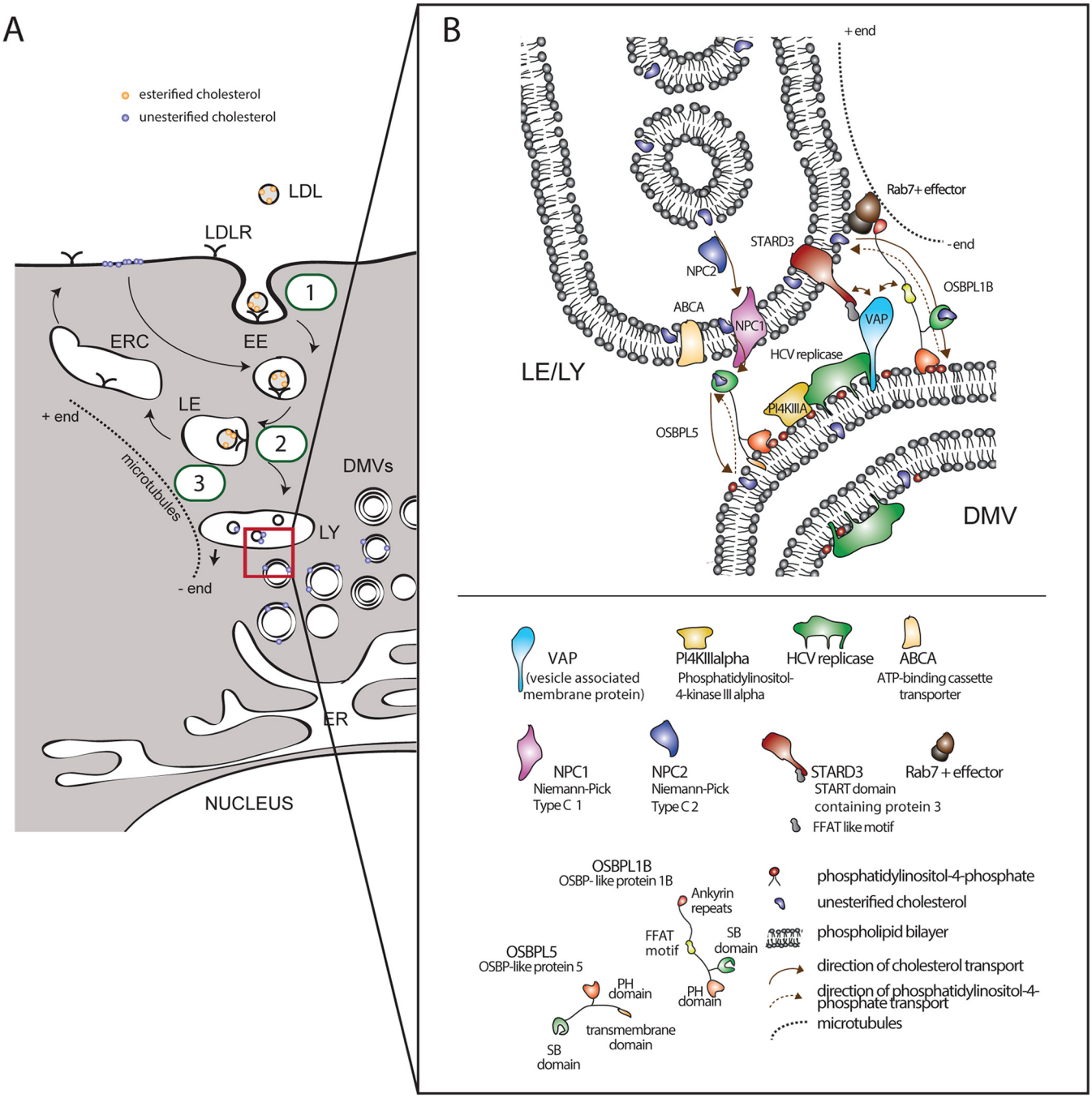

FIG 12 Possible mode of LTP-mediated cholesterol transport through the endocytic pathway to the viral replication sites. (A) Cholesterol-rich low-density lipoprotein (LDL) is taken up via receptor-mediated endocytosis and transported along the endosomal pathway to LE/LY (1). Through the activity of acid hydrolases, unesterified cholesterol is released from LDL (2) (80) and possibly transported over the LE/LY limiting membrane via the concerted action of several LTPs, such as NPC1/2, STARD3, OSBPL5, OSBPL1B (ORP1L), and ABCA. ORP1L regulates the localization of LE/LY according to their cholesterol content (3) (26, 52, 53). (B) HCV might take advantage of several of these LTPs to enrich cholesterol at the presumed viral replication sites, the DMVs. First, HCV recruits and activates PI4KIIIA, causing local accumulation of PI4P (16) and determining the directionality of lipid transfer by LTPs (15). Second, ER-resident VAP proteins present at DMVs (7) might serve as anchors for several proteins that promote the formation of ER-LE/LY membrane contact sites and direct lipid transfer. ORP1L regulating the mobility of LE/LY according to their cholesterol content is able to interact with VAP (26). It is likely that HCV redirects OSBPL1B (ORP1L) to bring cholesterol-loaded LE/LY membranes close to DMVs. The formation of these membrane contact sites might be promoted further by STARD3, another cholesterol efflux pump residing in the limiting membrane of late endosomes and interacting with VAP proteins (54). Once membrane contact site are established, NPC1, possibly in a concerted action with NPC2, catalyzes the export of unesterified cholesterol over the limiting membrane (22). The ER resident OSBPL5 (46, 47) or the cytosolic protein OSBP might then act as a cytosolic acceptor, possibly recruited by HCV. The high PI4P levels at DMVs most likely determine the directionality of cholesterol transport by OSBPL5 or OSBP (14), transferring the sterol to DMVs in exchange for PI4P. LDL, low-density lipoprotein; LDLR, low-density lipoprotein receptor; EE, early endosome; LE, late endosome; ERC, endosomal recycling compartment; DMVs, double-membrane vesicles; ER, endoplasmic reticulum.

factors important for efficient HCV replication (Fig. 1 and 12). These proteins are involved in cholesterol export and have been proposed to function at LE/LY membranes, similar to NPC1, although ABCA1 functions mainly at the PM (49–52). STARD3 and ABCA1 possibly act at different LE/LY pools and catalyze the export of cholesterol to distinct cellular targets, such as the PM or mitochondria (52, 53). Moreover, by binding to the ER-resident VAP proteins, STARD3 appears to contribute to the establishment of ER-LE membrane contact sites (54). Based on these considerations, we suggest that NPC1, possibly in a concerted action with STARD3 and OSBPL1B (ORP1L), is involved in the delivery of endosomal cholesterol to cytosolic sterol acceptors (Fig. 12). Interestingly, we (I. K. Stoeck and R. Bartenschlager, unpublished data) and others (14) observed that pharmacological inhibition of OSBP altered membranous web integrity. In line with this, we found that inhibition of endosomal cholesterol transport through treatment with cationic amphiphiles reduced DMV diameters and correlated with irregular DMV shape. Although we cannot rule out that decreased cholesterol amounts might make DMV membranes more fragile and thus more prone to EM preparation artifacts, our results suggest that cholesterol transport along the endosomal pathway is important for maintaining membranous web integrity. Whether cholesterol contributes solely to the morphology of DMVs or directly affects replicase activity, e.g., by providing lipid rafts (55), remains to be elucidated. Moreover, besides cholesterol, other lipids, such as sphingolipids and specific phospholipid species, appear to be relevant for viral replication and might be recruited in a similar manner (5).

Studying the role of cholesterol in viral RNA replication and the molecular details of its recruitment to the ROs has gained increasing attention in the field of RNA virology. For instance, endosomal cholesterol homeostasis was shown to be important for the replication of coxsackievirus B3 and encephalomyocarditis virus (56). In addition, rhinovirus was shown to utilize a PI4P-cholesterol countercurrent similar to that used by HCV (57). Moreover, imipramine, a drug causing the accumulation of cholesterol in LE/LY, reduces chikungunya virus, West Nile virus, Zika virus, and DENV replication (58). Thus, while the precise mechanisms of cholesterol recruitment may differ between various positive-strand RNA virus species, the dependency of viral replication on reshaping of the cellular cholesterol landscape seems to be a common feature for this large class of viruses. In this respect, studies of HCV hold great promise for gaining further insights into the complex interplay between positive-strand RNA viruses and intracellular lipid homeostasis.

MATERIALS AND METHODS

Antibodies. The following antibodies/reagents and respective dilutions were used in this study: alpha tubulin (1:1,000) (T6074; Sigma-Aldrich), beta actin (1:10,000) (A5441; Sigma-Aldrich), LAMP1 (1:100) (ab24170; Abcam), NPC1 (1:1,000) (AP60000PU-N; Acris), NS5A (1:1,000) (kindly provided by Charles Rice, Rockefeller University), and NS3 (1:1,000) (BioFront Technologies) antibodies, filipin III (250 μg/ml; Sigma-Aldrich), and Topfluor-cholesterol (1 μM; Avanti Polar Lipids). Secondary antibodies conjugated to horseradish peroxidase or to Alexa Fluor were purchased from Sigma-Aldrich or Thermo Fisher Scientific, respectively.

Cell culture, compounds, and cell viability assay. HEK-293T (59), Huh7.5 (60), Huh7.5FLuc (16) (cultured in the presence of 1 μg/ml Geneticin; Invitrogen), Huh7/Lunet (61), Huh7/LunetCD81H (62) (0.75 μg/ml Geneticin), Huh7/Lunet_LucUbiNeo_JFH1 (1 μg/ml Geneticin) (here designated LucUbiNeo-_JFH1), Huh7/Lunet_LucUbiNeo_Con1ET (0.5 μg/ml Geneticin) (here designated LucUbiNeo_Con1ET) (63, 64), Huh7/Lunet-T7 (5 μg/ml Zeocin) (65), Vero, and HeLa Kyoto cells were maintained in Dulbecco's modified Eagle medium (DMEM; Invitrogen, Karlsruhe, Germany) supplemented with 2 mM L-glutamine, nonessential amino acids, 100 U/ml penicillin, 100 μg/ml streptomycin, and 10% fetal calf serum (DMEMcplt). For some of these cell lines, antibiotics were added to the indicated final concentrations. In starvation experiments, cells were incubated in DMEM supplemented with 2 mM L-glutamine, nonessential amino acids, 100 U/ml penicillin, 100 μg/ml streptomycin, and 10% lipid-free fetal calf serum (c.c. pro GmbH) (LF-DMEM). U18666A was purchased from Sigma-Aldrich, and Ro 48-8071 was obtained from Enzo Life Sciences. Cell viability was measured by using the Cell Titer Glo luminescent-cell viability assay from Promega according to the manufacturer's protocol.

Plasmids and viral constructs. All nucleotide and amino acid numbers refer to the JFH-1 genome (GenBank accession no. AB047639) and the Con1 genome (GenBank accession no. AJ238799), respectively. Plasmids encoding the full-length chimera Jc1 (pFK-Jc1δg), the full-length *Renilla* luciferase reporter virus JcR2A (pFK_i389RLuc2a_Core_3-Jc1), the subgenomic reporter replicons pFK_i_341_PiLuc_NS3-3′H77S (genotype 1a), pFK_i389LucNS3-3′Con1ET_δg (genotype 1b), and pFK_i389Luc_NS3-

3′JFH1δg (genotype 2a), and the respective replication-deficient mutants pFK-i389-Luc_NS3-3ΔGDD_JFH1_δg and pFK_i389LucNS3-3′Con1ET_GND_δg were described previously (16, 66–69). The subgenomic reporter replicon constructs pSGR_S52/SG-Feo SHI (genotype 3a) and pSGR_ED43/SG-Feo VYG (genotype 4a) were kindly provided by Charles Rice, Rockefeller University, and have been described elsewhere (70). Plasmid pFK_DVs.R2A has been described previously (71). For lentivirus production, the retroviral vectors pCMV-dR8.91 and pMD2.G were used as described earlier (72, 73).

***In vitro* transcription and RNA transfection by electroporation.** To generate *in vitro* transcripts, 10 μg of the respective plasmid DNA was linearized by enzymatic digestion, purified, and used for *in vitro* transcription, using 80 mM HEPES (pH 7.5), 12 mM $MgCl_2$, 2 mM spermidine, 40 mM dithiothreitol (DTT), a 3.125 mM concentration of each nucleoside triphosphate, 1 U/μl of RNasin (Promega), and 0.6 U/μl of T7 RNA polymerase. Reactions were carried out at 37°C in a total volume of 100 μl. After 2 h, 0.3 U/μl of T7 RNA polymerase was added, and 4 h later, *in vitro* transcription was stopped by the addition of 2 U of RNase-free DNase (Promega) per μg DNA and 1 h of incubation at 37°C. After RNA purification by acidic phenol-chloroform extraction at 4°C, RNA was precipitated with isopropanol at room temperature. RNA pellets were dissolved in RNase-free water. The concentration of RNA was determined using a Nanodrop device (Thermo Fisher Scientific). For the transfection of target cells with the respective RNA, single-cell suspensions were washed with phosphate-buffered saline (PBS) and resuspended in Cytomix (74) containing 5 mM glutathione and 2 mM ATP. Four hundred or 100 μl of cell suspension was used for electroporation, using a Gene Pulser system (Bio-Rad) at 975 μF and 270 V for a 0.4-cm cuvette (Bio-Rad) or 500 μF and 166 V for a 0.2-cm cuvette (Bio-Rad), respectively.

Lentivirus preparation and titration. HEK-293T cells were transfected with packaging (pCMV-dR8.91) and envelope (pMD2.G) plasmids (72, 73) as well as a transfer plasmid (pLKO.1; Sigma-Aldrich) encoding the desired shRNA by use of polyethylenimine (Polysciences Inc.). Supernatants were harvested at 48 h and 72 h posttransfection and filtered, and virus titers were determined by a colony formation assay. For this purpose, HeLa Kyoto cells were transduced with two different dilutions of the lentivirus stock, and 24 h later, cells were subjected to selection by culture in medium containing 1 μg/ml puromycin (Sigma-Aldrich). Nontransduced cells served as a control for the selection procedure. Cell colonies were visualized with crystal violet and counted.

Immunoblotting. Samples were harvested in 1 volume of 6× SDS sample buffer (375 mM Tris-HCl [pH 6.8], 0.1% [wt/vol] bromophenol blue, 20% glycerol, 3% [wt/vol] SDS, 2% [vol/vol] beta-mercaptoethanol) and 5 volumes of PBS and denatured by heating at 95°C for 5 min. Proteins were analyzed by SDS-polyacrylamide gel electrophoresis followed by semidry electrotransfer onto polyvinylidene difluoride (PVDF) membranes (PerkinElmer Life Sciences). For immunodetection of NPC1, proteins were separated in a 6% SDS-polyacrylamide gel, followed by overnight wet transfer onto PVDF membranes at 4°C. Membranes were blocked in 5% skim milk dissolved in PBS-Tween 20 (0.5%) for 1 h at room temperature and then incubated with the appropriate primary antibody solution (containing 2.5% skim milk) overnight at 4°C. The membranes were then washed with PBS-Tween 20 (3 times for 10 min each) and incubated with the secondary antibody solution (containing 2.5% skim milk) for 1 h at room temperature. Membranes were washed with PBS-Tween 20 (3 times for 10 min each), followed by a final wash with PBS (5 min). Membranes were developed by using Western Lightning Plus ECL reagent (PerkinElmer) and an Intas Science imager.

Immunofluorescence microscopy and image analysis. For indirect immunofluorescence assay, cells were grown on coverslips and washed once with PBS prior to fixation with 4% paraformaldehyde (PFA) in PBS for 15 min at room temperature. Given that filipin itself permeabilizes the cell, additional permeabilization was not necessary. Primary and secondary antibodies were incubated in the presence of 250 μg/ml filipin III (here designated filipin) for 1 h each (75). Cells were washed with PBS and mounted with Vectashield (Vector Laboratories Inc.). Images were analyzed using a Leica Sp2 confocal laser scanning microscope or a PerkinElmer ERS-6 spinning disc confocal microscope. To quantify the volume of filipin-positive structures, z-stacks were captured to cover the complete cell volume. Images were deconvolved using Autoquant X3 software (Bitplane), and volumes were measured using Imaris 8 software (Bitplane). The colocalization of two signals was determined by performing intensity correlation analysis using the Fiji software package based on ImageJ (NIH). The signal intensity was determined by measuring the respective integrated density by use of Fiji.

Live-cell imaging. Huh7/LunetCD81H cells stably expressing the HCV polyprotein fragment from core to NS2 of the Jc1 isolate were electroporated with *in vitro* transcripts of subgenomic replicon RNA encoding a fully functional mCherry-tagged NS5A protein (genotype 2a; isolate JFH1) (subg_NS5AmCherry) (35). Cells were plated into 8-well Lab-Tek imaging chambers (Thermo Fisher Scientific), and Topfluor-cholesterol (1 μM) was added for 10 min prior to imaging. After extensive washing with phenol red-free imaging medium, live-cell imaging was performed using a PerkinElmer ERS-6 spinning disc confocal microscope and an incubation chamber at 37°C and 5% CO_2. Every 15 min, the cell volume was acquired by imaging sequential z-stacks. In order to stain for lipid droplets, LipidTox Deep Red neutral lipid stain (Thermo Fisher Scientific) was directly added to the cells at a final dilution of 1:1,000 at the end of the imaging period. After 20 min, cells were imaged for approximately 45 min, which allowed acquisition of 3 additional frames.

Sample preparation and analysis by TEM. Cells seeded onto coverslips were washed with PBS and fixed for 30 min at room temperature with 2.5% glutaraldehyde in a 50 mM sodium cacodylate (caco) buffer (pH 7.2) containing 10 mM $MgCl_2$, 10 mM $CaCl_2$, 100 mM KCl, and 2% sucrose. Cells were rinsed with caco buffer five times for 5 min each on ice prior to incubation with 2% osmium tetroxide in caco buffer for 40 min on ice. Samples were rinsed with distilled water and left in 0.5% uranyl acetate overnight at 4°C. Next, samples were washed with distilled water for 30 min, and dehydration was

performed by sequential incubation with ethanol at different concentrations (40%, 50%, 60%, 70%, and 80% for 5 min each and 95% and 100% for 20 min each). Samples were embedded in an araldite-Epon mixture (Araldite 502/Embed 812 kit; Electron Microscopy Sciences) and left for 2 days at 60°C for polymerization. After removal of the coverslip, embedded cells were cut into 70-nm sections by use of a Leica Ultracut UCT microtome and a diamond knife and mounted onto a mesh grid. The retrieved sections were further incubated with 3% uranyl acetate in 70% methanol for 5 min, followed by 2% lead citrate in distilled water for 2 min. Sections were analyzed using a JEOL JEM1400 transmission electron microscope (TEM) (JEOL Ltd., Tokyo, Japan) provided by the Electron Microscopy Core Facility of Heidelberg University.

CLEM. For correlative light electron microscopy (CLEM), cells were seeded onto glass-bottomed culture dishes containing gridded coverslips (MatTek Corporation). After 48 h, cells were fixed with 4% PFA and 0.2% glutaraldehyde in PBS for 30 min at room temperature, washed three times with PBS, and analyzed with a PerkinElmer ERS-6 spinning disc confocal microscope to acquire optical sections of 0.2 μm. Fluorescence signals from transfected cells and their positions on the gridded coverslip were recorded. After imaging, cells were fixed again and processed as described in the section above, with the exception that sections were collected on slot grids. Sections were imaged by using a JEOL JEM1400 TEM. To correlate light and electron microscopy images, the "landmark correspondences" plug-in of the Fiji software package was used.

Luciferase reporter activity assay. The effect of drug treatment or RNAi-mediated knockdown on viral replication was determined by measuring the *Renilla* luciferase reporter activity in cell lysates of *Renilla* reporter virus-infected cells. The firefly luciferase activity in cell lysates containing the subgenomic firefly luciferase reporter replicon was measured accordingly. To measure luciferase activity, the respective substrates were added to the cell lysates (coelenterazine for *Renilla* luciferase and luciferine, glycyl-glycine, ATP, and dithiothreitol for firefly luciferase), and emitted light was quantified using either a Lumat LB9507 tube luminometer or a Mithras LB940 plate luminometer (both from Berthold Technologies).

Generation of CRISPR/Cas9 NPC1 KO or control cell lines. The following 4 20-base guide strands (strands 1 to 4) were designed to target different exons in the NPC1 gene: strand 1, 5′-GAATTGCATAT GGGGACAAG-3′; strand 2, 5′-AAAGAGTTACAATACTACGT-3′; strand 3, 5′-CACAAGCAAAAACGCCATGT-3′; and strand 4, 5′-CAACTGGATTGGTTGTGACC-3′. CRISPR plasmids were constructed by insertion of the annealed oligonucleotides into the lentiCRIPSRv2 plasmid (Addgene). In this vector, the single guide RNAs are transcribed under the control of the U6 promoter. Lentiviruses were prepared as described above. To generate knockout cell lines, Huh7-Lunet cells were infected with the respective lentivirus, and 1 day later, cells were cultured in medium containing 3 μg/ml puromycin. Two days later, the obtained cell pools were used for the experiments.

CRISPR/Cas9 assay. Lunet CRISPR/Cas9 KO or control cell pools were electroporated with *in vitro* transcripts of the full-length *Renilla* luciferase reporter virus and seeded into 12-well plates. Cells were harvested after 4 h to determine transfection efficiency and after 48 h to assess virus replication, whereas cell culture supernatant was transferred onto naive Huh7.5 cells to determine the impact of NPC1 knockout on virus production.

RNAi screen. Six independent repetitions were performed, each time using a different plate layout; 2.5 μl of 100 μM siRNA On-Target Plus SMART pool (Dharmacon) was transfected by electroporation into Huh7.5FLuc cells. For controls, several electroporations of the siRNAs were included (5 for the nontargeting siRNA, 2 for the ApoE siRNA, and 2 for the PI4KIIIA siRNA), while for the remaining siRNAs, only a single electroporation was performed per biological replicate. Cells were seeded in triplicate into 96-well plates and infected either 36 h (HCV reporter genome JcR2A) (16) or 48 h (DENV reporter genome DVR2A) (71) later with the respective *Renilla* luciferase reporter virus at a multiplicity of infection (MOI) of 0.5. After 24 h, the inoculum was replaced with 100 μl of fresh DMEMcplt. In the case of DENV infection, 10 mM HEPES buffer solution (Thermo Fisher Scientific) was added to the medium. After 60 h (HCV) or 48 h (DENV), cell supernatants were transferred onto naive Huh7.5 cells (HCV) or Vero cells (DENV) seeded 1 day prior to infection. Infection was stopped 48 h later by washing and lysis of cells (1% [vol/vol] Triton X-100, 10% glycerol, 15 mM $MgSO_4$, 4 mM EGTA, 25 mM glycyl-glycine [pH 7.8], 1 mM DTT). Luciferase activity was measured as a readout for viral RNA replication.

siRNA and shRNA. The following siRNA On-Target Plus SMART pools (pool numbers) were ordered from Dharmacon: OSBP (L-009747-00), OSBPL1A/B (L-008350-00), OSBPL2 (L-010361-01), OSBPL3 (L-009380-01), OSBPL5 (L-009274-01), OSBPL6 (L-009437-01), OSBPL8 (L-009508-00), OSBPL9 (L-009912-00), OSBPL10 (L-008409-00), OSBPL11 (L-008415-01), PLEKHA8 (L-004320-01), COL4A3BP (L-012101-00), STARD3 (L-017665-00), STARD4 (L-003315-01), NPC1 (L-008047-00), NPC2 (L-017216-00), ABCA1 (L-004128-00), PI4KA (L-006776-00), APOE (L-006470-00), and *Renilla* luciferase (CTM-27030) pools. The following Mission shRNA bacterial glycerol stocks were ordered from Sigma-Aldrich and used for lentivirus production: for ApoE, CCGGGACAATCACTGAACGCCGAAGCTCGAGCTTCGGCGTTCAGTGATTGT CTTTTTG; for PI4KIIIA, CCGGCAAGGCTGGATCAACACATACCTCGAGGTATGTGTTGATCCAGCCTTGTTTTTG; for NPC1, CCGGCCACAAGTTCTATACCATATTCTCGAGAATATGGTATAGAACTTGTGGTTTTT and CCGGAGAG GTACAATTGCGAATATTCTCGAGAATATTCGCAATTGTACCTCTTTTTTTG; for STARD3, CCGGGACCTGGTTCCT TGACTTCAACTCGAGTTGAAGTCAAGGAACCAGGTCTTTTTG and CCGGCAGGAAGAGAACTGGAAGTTTCTCG AGAAACTTCCAGTTCTCTTCCTGTTTTTTG; for OSBPL1A/B, CCGGGCATCAAGAAACACAGAACAACTCGAGTT GTTCTGTGTTTCTTGATGCTTTTTTG and CCGGGCCGGATTCTGAAAGTGTATTCTCGAGAATACACTTTCAGAAT CCGGCTTTTTTG; nontargeting 1, CCGGCAACAAGATGAAGAGCACCAACTCGAGTTGGTGCTCTTCATCTTGTT GTTTTT; and nontargeting 2, CCGGCAACAAGATGAAGAGCACCAACTCGAGTTGGTGCTCTTCATCTTGTG TTTTT.

Statistical analysis of the RNAi screen. Screening data were analyzed in R by using the RNAither package (76). In brief, technical replicates were averaged using the mean. Platewise Z-scores were computed by subtracting the mean and dividing by the standard deviation for the nontargeting negative controls. Biological replicates were summarized, and statistical significance was determined using a one-sample *t* test.

Dose-response assays. For dose-response assays, Huh7/Lunet cells were electroporated with 10 μg *in vitro* transcripts of the HCV *Renilla* reporter virus JcR2A or with 5 μg of subgenomic reporter replicon RNA. Cells were seeded into 96-well plates, and 4 h later, the medium was replaced with fresh medium, with or without the respective drug. After 24, 48, or 96 h, cells were lysed and used to measure luciferase activity. To assess the efficiency of HCV particle production, we had to rule out an impact of the drug on virus particle infectivity or on virus entry. Therefore, the culture supernatant was removed, and after washing, cells were incubated in DMEMcplt for 4 h at 37°C. Infectious particles produced during those 4 h were harvested and used for infection of naive Huh7.5 cells. Infection efficiency was determined by measuring the luciferase activity in lysates of these cells prepared 48 h after infection. For dose-response assays conducted with stable replicon cell lines, 1×10^4 LucUbiNeo_JFH1- or LucUbiNeo_Con1ET-containing cells were seeded per well of a 96-well plate. One day later, cells were incubated with control medium or medium containing given concentrations of the drug. Cells were harvested 48, 72, and 96 h posttreatment, and effects on replication were assessed by luciferase assay as described earlier.

Preparation of virus stocks and virus titration. Huh7.5 cells were transfected with *in vitro* transcripts of wild-type Jc1 or JcR2A by electroporation. After 24 h, supernatants were replaced with fresh medium, and at 48, 72, and 96 h postelectroporation, supernatants were collected and filtered through 0.45-μm-pore-size filters. Supernatants were stored at −70°C prior to determination of virus titers by limiting dilution assay. For this purpose, Huh7.5 cells were seeded into 96-well plates, and serial dilutions of the virus stock were used for infection. Infected cells were detected by immunohistochemistry using the NS3-specific antibody 2E3, and the 50% tissue culture infective dose ($TCID_{50}$) was determined using the method of Spearman and Kärber (77, 78). The preparation of dengue virus stocks has been described elsewhere (71).

Total cellular RNA isolation and quantification by RT-qPCR. Isolation of total cellular RNA was carried out using a NucleoSpin RNA extraction kit (Macherey-Nagel). Typically, 350 μl of buffer A1 supplemented with 1% beta-mercaptoethanol was added to a confluent well of a 24-well plate, and RNA was prepared as recommended by the manufacturer. To generate cDNA from isolated RNA, a high-capacity cDNA reverse transcription (RT) kit (Thermo Scientific) was used. The 2× reaction mixture contained 2× RT buffer, a deoxynucleoside triphosphate (dNTP) mixture containing a 4 mM concentration of each dNTP, 2× RT random primer, 25 U reverse transcriptase, and RNase inhibitor and was added to the isolated RNA. The reaction mixture was incubated in a Thermocycler (Eppendorf) using the following program: 10 min at 25°C, 120 min at 37°C, 5 min at 85°C, and storage at 4°C. The cDNA was diluted 1:10 in RNase-free water and directly used for quantitative PCR (qPCR), using an iTaq Universal SYBR green kit (Bio-Rad). A master mix (12 μl/sample) consisting of 2× iTaq Universal mix (Bio-Rad) and 0.5 μM (each) corresponding sense and antisense primers was prepared, to which 3 μl of prediluted cDNA was added. Each reaction was conducted in triplicate. mRNA levels for NPC1 and glyceraldehyde-3-phosphate dehydrogenase (GAPDH) were determined using the following primer pairs: NPC1-fwd, 5′-TTGTGGTGTTGGCTTTTGCC-3′; NPC1-rev, 5′-TGGCTTTATTTACTGATGGCCCTAT-3′; GAPDH-fwd, 5′-GAA GGTGAAGGTCGGAGTC-3′; and GAPDH-rev, 5′-GAAGATGGTGATGGGATTC-3′.

Starvation assays. Huh7 cells containing the LucUbiNeo_Con1ET or LucUbiNeo_JFH1 replicon were seeded in triplicate for each condition in 96-well plates. After 24 h, cells were transferred to LF-DMEM, and 6 h later, the medium was replaced with fresh LF-DMEM without or with 50 μg/ml human LDL (Merck Millipore).

Statistical analysis. Statistical analysis was performed using the GraphPad Prism 6 software package (GraphPad Software Inc.). Significance values were calculated using two-tailed, unpaired Student's *t* test.

SUPPLEMENTAL MATERIAL

Supplemental material for this article may be found at https://doi.org/10.1128/JVI.01196-17.

SUPPLEMENTAL FILE 1, AVI file, 1.2 MB.

SUPPLEMENTAL FILE 2, AVI file, 2.3 MB.

SUPPLEMENTAL FILE 3, PDF file, 0.1 MB.

ACKNOWLEDGMENTS

We thank Uta Haselmann, Ulrike Herian, Stephanie Kallis, Marie Bartenschlager, and Fredy Huschmand for their continuous help and support and Vibor Laketa from the Infectious Diseases Imaging Platform (IDIP) and Stefan Hillmer from the Electron Microscopy Core Facility (EMCF Heidelberg) for their excellent assistance and support in imaging. We further acknowledge the members of the Molecular Virology Unit for stimulating feedback on this work, especially Margarita Zayas, Marion Poenisch, Carola Berger, and Laurent Chatel-Chaix.

This work was supported by the Deutsche Forschungsgemeinschaft (grants TRR83,

TP13, and SFB1129, TP11, both to R.B.). L.K. was supported by the Bundesministerium für Bildung und Forschung (BMBF) (ERANET ERASysApp SysVirDrug) (grant 031A602A).

REFERENCES

1. World Health Organization. 2017. Global hepatitis report, 2017. World Health Organization, Geneva, Switzerland. http://www.who.int/hepatitis/publications/global-hepatitis-report2017/en/.
2. Deuffic-Burban S, Poynard T, Sulkowski MS, Wong JB. 2007. Estimating the future health burden of chronic hepatitis C and human immunodeficiency virus infections in the United States. J Viral Hepat 14:107–115. https://doi.org/10.1111/j.1365-2893.2006.00785.x.
3. Bartenschlager R, Lohmann V, Penin F. 2013. The molecular and structural basis of advanced antiviral therapy for hepatitis C virus infection. Nat Rev Microbiol 11:482–496. https://doi.org/10.1038/nrmicro3046.
4. Paul D, Bartenschlager R. 2013. Architecture and biogenesis of plus-strand RNA virus replication factories. World J Virol 2:32–48. https://doi.org/10.5501/wjv.v2.i2.32.
5. Paul D, Madan V, Bartenschlager R. 2014. Hepatitis C virus RNA replication and assembly: living on the fat of the land. Cell Host Microbe 16:569–579. https://doi.org/10.1016/j.chom.2014.10.008.
6. Romero-Brey I, Merz A, Chiramel A, Lee JY, Chlanda P, Haselman U, Santarella-Mellwig R, Habermann A, Hoppe S, Kallis S, Walther P, Antony C, Krijnse-Locker J, Bartenschlager R. 2012. Three-dimensional architecture and biogenesis of membrane structures associated with hepatitis C virus replication. PLoS Pathog 8:e1003056. https://doi.org/10.1371/journal.ppat.1003056.
7. Paul D, Hoppe S, Saher G, Krijnse-Locker J, Bartenschlager R. 2013. Morphological and biochemical characterization of the membranous hepatitis C virus replication compartment. J Virol 87:10612–10627. https://doi.org/10.1128/JVI.01370-13.
8. Romero-Brey I, Berger C, Kallis S, Kolovou A, Paul D, Lohmann V, Bartenschlager R. 2015. NS5A domain 1 and polyprotein cleavage kinetics are critical for induction of double-membrane vesicles associated with hepatitis C virus replication. mBio 6:e00759. https://doi.org/10.1128/mBio.00759-15.
9. Nagy PD, Strating JR, van Kuppeveld FJ. 2016. Building viral replication organelles: close encounters of the membrane types. PLoS Pathog 12:e1005912. https://doi.org/10.1371/journal.ppat.1005912.
10. Aizaki H, Lee KJ, Sung VM, Ishiko H, Lai MM. 2004. Characterization of the hepatitis C virus RNA replication complex associated with lipid rafts. Virology 324:450–461. https://doi.org/10.1016/j.virol.2004.03.034.
11. Shi ST, Lee KJ, Aizaki H, Hwang SB, Lai MM. 2003. Hepatitis C virus RNA replication occurs on a detergent-resistant membrane that cofractionates with caveolin-2. J Virol 77:4160–4168. https://doi.org/10.1128/JVI.77.7.4160-4168.2003.
12. Holthuis JC, Menon AK. 2014. Lipid landscapes and pipelines in membrane homeostasis. Nature 510:48–57. https://doi.org/10.1038/nature13474.
13. Amako Y, Sarkeshik A, Hotta H, Yates J, III, Siddiqui A. 2009. Role of oxysterol binding protein in hepatitis C virus infection. J Virol 83:9237–9246. https://doi.org/10.1128/JVI.00958-09.
14. Wang H, Perry JW, Lauring AS, Neddermann P, De FR, Tai AW. 2014. Oxysterol-binding protein is a phosphatidylinositol 4-kinase effector required for HCV replication membrane integrity and cholesterol trafficking. Gastroenterology 146:1373–1385. https://doi.org/10.1053/j.gastro.2014.02.002.
15. Mesmin B, Bigay J, Moser von Filseck J, Lacas-Gervais S, Drin G, Antonny B. 2013. A four-step cycle driven by PI(4)P hydrolysis directs sterol/PI(4)P exchange by the ER-Golgi tether OSBP. Cell 155:830–843. https://doi.org/10.1016/j.cell.2013.09.056.
16. Reiss S, Rebhan I, Backes P, Romero-Brey I, Erfle H, Matula P, Kaderali L, Poenisch M, Blankenburg H, Hiet MS, Longerich T, Diehl S, Ramirez F, Balla T, Rohr K, Kaul A, Buhler S, Pepperkok R, Lengauer T, Albrecht M, Eils R, Schirmacher P, Lohmann V, Bartenschlager R. 2011. Recruitment and activation of a lipid kinase by hepatitis C virus NS5A is essential for integrity of the membranous replication compartment. Cell Host Microbe 9:32–45. https://doi.org/10.1016/j.chom.2010.12.002.
17. Berger KL, Cooper JD, Heaton NS, Yoon R, Oakland TE, Jordan TX, Mateu G, Grakoui A, Randall G. 2009. Roles for endocytic trafficking and phosphatidylinositol 4-kinase III alpha in hepatitis C virus replication. Proc Natl Acad Sci U S A 106:7577–7582. https://doi.org/10.1073/pnas.0902693106.
18. Khan I, Katikaneni DS, Han Q, Sanchez-Felipe L, Hanada K, Ambrose RL, Mackenzie JM, Konan KV. 2014. Modulation of hepatitis C virus genome replication by glycosphingolipids and four-phosphate adaptor protein 2. J Virol 88:12276–12295. https://doi.org/10.1128/JVI.00970-14.
19. Lehto M, Olkkonen VM. 2003. The OSBP-related proteins: a novel protein family involved in vesicle transport, cellular lipid metabolism, and cell signalling. Biochim Biophys Acta 1631:1–11. https://doi.org/10.1016/S1388-1981(02)00364-5.
20. Clark BJ. 2012. The mammalian START domain protein family in lipid transport in health and disease. J Endocrinol 212:257–275. https://doi.org/10.1530/JOE-11-0313.
21. D'Angelo G, Polishchuk E, Di TG, Santoro M, Di CA, Godi A, West G, Bielawski J, Chuang CC, van der Spoel AC, Platt FM, Hannun YA, Polishchuk R, Mattjus P, De Matteis MA. 2007. Glycosphingolipid synthesis requires FAPP2 transfer of glucosylceramide. Nature 449:62–67. https://doi.org/10.1038/nature06097.
22. Infante RE, Wang ML, Radhakrishnan A, Kwon HJ, Brown MS, Goldstein JL. 2008. NPC2 facilitates bidirectional transfer of cholesterol between NPC1 and lipid bilayers, a step in cholesterol egress from lysosomes. Proc Natl Acad Sci U S A 105:15287–15292. https://doi.org/10.1073/pnas.0807328105.
23. Lev S. 2004. The role of the Nir/rdgB protein family in membrane trafficking and cytoskeleton remodeling. Exp Cell Res 297:1–10. https://doi.org/10.1016/j.yexcr.2004.02.033.
24. Chang KS, Jiang J, Cai Z, Luo G. 2007. Human apolipoprotein E is required for infectivity and production of hepatitis C virus in cell culture. J Virol 81:13783–13793. https://doi.org/10.1128/JVI.01091-07.
25. Strauss JF, Kishida T, III, Christenson LK, Fujimoto T, Hiroi H. 2003. START domain proteins and the intracellular trafficking of cholesterol in steroidogenic cells. Mol Cell Endocrinol 202:59–65. https://doi.org/10.1016/S0303-7207(03)00063-7.
26. Rocha N, Kuijl C, van der Kant R, Janssen L, Houben D, Janssen H, Zwart W, Neefjes J. 2009. Cholesterol sensor ORP1L contacts the ER protein VAP to control Rab7-RILP-p150 Glued and late endosome positioning. J Cell Biol 185:1209–1225. https://doi.org/10.1083/jcb.200811005.
27. Carette JE, Raaben M, Wong AC, Herbert AS, Obernosterer G, Mulherkar N, Kuehne AI, Kranzusch PJ, Griffin AM, Ruthel G, Dal CP, Dye JM, Whelan SP, Chandran K, Brummelkamp TR. 2011. Ebola virus entry requires the cholesterol transporter Niemann-Pick C1. Nature 477:340–343. https://doi.org/10.1038/nature10348.
28. Kato T, Date T, Miyamoto M, Furusaka A, Tokushige K, Mizokami M, Wakita T. 2003. Efficient replication of the genotype 2a hepatitis C virus subgenomic replicon. Gastroenterology 125:1808–1817. https://doi.org/10.1053/j.gastro.2003.09.023.
29. Krieger N, Lohmann V, Bartenschlager R. 2001. Enhancement of hepatitis C virus RNA replication by cell culture-adaptive mutations. J Virol 75:4614–4624. https://doi.org/10.1128/JVI.75.10.4614-4624.2001.
30. Lu F, Liang Q, Abi-Mosleh L, Das A, De Brabander JK, Goldstein JL, Brown MS. 2015. Identification of NPC1 as the target of U18666A, an inhibitor of lysosomal cholesterol export and Ebola infection. eLife 4:e12177. https://doi.org/10.7554/eLife.12177.
31. Shoemaker CJ, Schornberg KL, Delos SE, Scully C, Pajouhesh H, Olinger GG, Johansen LM, White JM. 2013. Multiple cationic amphiphiles induce a Niemann-Pick C phenotype and inhibit Ebola virus entry and infection. PLoS One 8:e56265. https://doi.org/10.1371/journal.pone.0056265.
32. Koutsoudakis G, Herrmann E, Kallis S, Bartenschlager R, Pietschmann T. 2007. The level of CD81 cell surface expression is a key determinant for productive entry of hepatitis C virus into host cells. J Virol 81:588–598. https://doi.org/10.1128/JVI.01534-06.
33. Schroeder F, Holland JF, Bieber LL. 1971. Fluorometric evidence for the binding of cholesterol to the filipin complex. J Antibiot (Tokyo) 24:846–849. https://doi.org/10.7164/antibiotics.24.846.
34. Holtta-Vuori M, Uronen RL, Repakova J, Salonen E, Vattulainen I, Panula P, Li Z, Bittman R, Ikonen E. 2008. BODIPY-cholesterol: a new tool to visualize sterol trafficking in living cells and organisms. Traffic 9:1839–1849. https://doi.org/10.1111/j.1600-0854.2008.00801.x.
35. Ruggieri A, Dazert E, Metz P, Hofmann S, Bergeest JP, Mazur J, Bankhead P, Hiet MS, Kallis S, Alvisi G, Samuel CE, Lohmann V, Kaderali L, Rohr K, Frese M, Stoecklin G, Bartenschlager R. 2012. Dynamic oscillation of

translation and stress granule formation mark the cellular response to virus infection. Cell Host Microbe 12:71–85. https://doi.org/10.1016/j.chom.2012.05.013.
36. Zayas M, Long G, Madan V, Bartenschlager R. 2016. Coordination of hepatitis C virus assembly by distinct regulatory regions in nonstructural protein 5A. PLoS Pathog 12:e1005376. https://doi.org/10.1371/journal.ppat.1005376.
37. Vanier MT. 2010. Niemann-Pick disease type C. Orphanet J Rare Dis 5:16. https://doi.org/10.1186/1750-1172-5-16.
38. Morand OH, Aebi JD, Dehmlow H, Ji YH, Gains N, Lengsfeld H, Himber J. 1997. Ro 48-8.071, a new 2,3-oxidosqualene:lanosterol cyclase inhibitor lowering plasma cholesterol in hamsters, squirrel monkeys, and minipigs: comparison to simvastatin. J Lipid Res 38:373–390.
39. Cenedella RJ. 2009. Cholesterol synthesis inhibitor U18666A and the role of sterol metabolism and trafficking in numerous pathophysiological processes. Lipids 44:477–487. https://doi.org/10.1007/s11745-009-3305-7.
40. Elgner F, Ren H, Medvedev R, Ploen D, Himmelsbach K, Boller K, Hildt E. 2016. The intracellular cholesterol transport inhibitor U18666A inhibits the exosome-dependent release of mature hepatitis C virus. J Virol 90:11181–11196. https://doi.org/10.1128/JVI.01053-16.
41. Mukherjee S, Maxfield FR. 2004. Lipid and cholesterol trafficking in NPC. Biochim Biophys Acta 1685:28–37. https://doi.org/10.1016/j.bbalip.2004.08.009.
42. Wang H, Tai AW. 2017. Continuous de novo generation of spatially segregated hepatitis C virus replication organelles revealed by pulse-chase imaging. J Hepatol 66:55–66. https://doi.org/10.1016/j.jhep.2016.08.018.
43. Evans MJ, Rice CM, Goff SP. 2004. Phosphorylation of hepatitis C virus nonstructural protein 5A modulates its protein interactions and viral RNA replication. Proc Natl Acad Sci U S A 101:13038–13043. https://doi.org/10.1073/pnas.0405152101.
44. Gao L, Aizaki H, He JW, Lai MM. 2004. Interactions between viral nonstructural proteins and host protein hVAP-33 mediate the formation of hepatitis C virus RNA replication complex on lipid raft. J Virol 78:3480–3488. https://doi.org/10.1128/JVI.78.7.3480-3488.2004.
45. Hamamoto I, Nishimura Y, Okamoto T, Aizaki H, Liu M, Mori Y, Abe T, Suzuki T, Lai MM, Miyamura T, Moriishi K, Matsuura Y. 2005. Human VAP-B is involved in hepatitis C virus replication through interaction with NS5A and NS5B. J Virol 79:13473–13482. https://doi.org/10.1128/JVI.79.21.13473-13482.2005.
46. Du X, Kumar J, Ferguson C, Schulz TA, Ong YS, Hong W, Prinz WA, Parton RG, Brown AJ, Yang H. 2011. A role for oxysterol-binding protein-related protein 5 in endosomal cholesterol trafficking. J Cell Biol 192:121–135. https://doi.org/10.1083/jcb.201004142.
47. Du X, Yang H. 2013. Endosomal cholesterol trafficking: protein factors at a glance. Acta Biochim Biophys Sin (Shanghai) 45:11–17. https://doi.org/10.1093/abbs/gms095.
48. Pu J, Guardia CM, Keren-Kaplan T, Bonifacino JS. 2016. Mechanisms and functions of lysosome positioning. J Cell Sci 129:4329–4339. https://doi.org/10.1242/jcs.196287.
49. Boadu E, Francis GA. 2006. The role of vesicular transport in ABCA1-dependent lipid efflux and its connection with NPC pathways. J Mol Med (Berl) 84:266–275. https://doi.org/10.1007/s00109-005-0001-9.
50. Boadu E, Nelson RC, Francis GA. 2012. ABCA1-dependent mobilization of lysosomal cholesterol requires functional Niemann-Pick C2 but not Niemann-Pick C1 protein. Biochim Biophys Acta 1821:396–404. https://doi.org/10.1016/j.bbalip.2011.11.013.
51. Neufeld EB, Remaley AT, Demosky SJ, Stonik JA, Cooney AM, Comly M, Dwyer NK, Zhang M, Blanchette-Mackie J, Santamarina-Fojo S, Brewer HB, Jr. 2001. Cellular localization and trafficking of the human ABCA1 transporter. J Biol Chem 276:27584–27590. https://doi.org/10.1074/jbc.M103264200.
52. van der Kant R, Zondervan I, Janssen L, Neefjes J. 2013. Cholesterol-binding molecules MLN64 and ORP1L mark distinct late endosomes with transporters ABCA3 and NPC1. J Lipid Res 54:2153–2165. https://doi.org/10.1194/jlr.M037325.
53. Charman M, Kennedy BE, Osborne N, Karten B. 2010. MLN64 mediates egress of cholesterol from endosomes to mitochondria in the absence of functional Niemann-Pick type C1 protein. J Lipid Res 51:1023–1034. https://doi.org/10.1194/jlr.M002345.
54. Wilhelm LP, Tomasetto C, Alpy F. 2016. Touche! STARD3 and STARD3NL tether the ER to endosomes. Biochem Soc Trans 44:493–498. https://doi.org/10.1042/BST20150269.
55. Weng L, Hirata Y, Arai M, Kohara M, Wakita T, Watashi K, Shimotohno K, He Y, Zhong J, Toyoda T. 2010. Sphingomyelin activates hepatitis C virus RNA polymerase in a genotype-specific manner. J Virol 84:11761–11770. https://doi.org/10.1128/JVI.00638-10.
56. Albulescu L, Wubbolts R, van Kuppeveld FJ, Strating JR. 2015. Cholesterol shuttling is important for RNA replication of coxsackievirus B3 and encephalomyocarditis virus. Cell Microbiol 17:1144–1156. https://doi.org/10.1111/cmi.12425.
57. Roulin PS, Lotzerich M, Torta F, Tanner LB, van Kuppeveld FJ, Wenk MR, Greber UF. 2014. Rhinovirus uses a phosphatidylinositol 4-phosphate/cholesterol counter-current for the formation of replication compartments at the ER-Golgi interface. Cell Host Microbe 16:677–690. https://doi.org/10.1016/j.chom.2014.10.003.
58. Wichit S, Hamel R, Bernard E, Talignani L, Diop F, Ferraris P, Liegeois F, Ekchariyawat P, Luplertlop N, Surasombatpattana P, Thomas F, Merits A, Choumet V, Roques P, Yssel H, Briant L, Misse D. 2017. Imipramine inhibits chikungunya virus replication in human skin fibroblasts through interference with intracellular cholesterol trafficking. Sci Rep 7:3145. https://doi.org/10.1038/s41598-017-03316-5.
59. Graham FL, Smiley J, Russell WC, Nairn R. 1977. Characteristics of a human cell line transformed by DNA from human adenovirus type 5. J Gen Virol 36:59–74. https://doi.org/10.1099/0022-1317-36-1-59.
60. Blight KJ, McKeating JA, Rice CM. 2002. Highly permissive cell lines for subgenomic and genomic hepatitis C virus RNA replication. J Virol 76:13001–13014. https://doi.org/10.1128/JVI.76.24.13001-13014.2002.
61. Friebe P, Boudet J, Simorre JP, Bartenschlager R. 2005. Kissing-loop interaction in the 3′ end of the hepatitis C virus genome essential for RNA replication. J Virol 79:380–392. https://doi.org/10.1128/JVI.79.1.380-392.2005.
62. Koutsoudakis G, Kaul A, Steinmann E, Kallis S, Lohmann V, Pietschmann T, Bartenschlager R. 2006. Characterization of the early steps of hepatitis C virus infection by using luciferase reporter viruses. J Virol 80:5308–5320. https://doi.org/10.1128/JVI.02460-05.
63. Lohmann V, Hoffmann S, Herian U, Penin F, Bartenschlager R. 2003. Viral and cellular determinants of hepatitis C virus RNA replication in cell culture. J Virol 77:3007–3019. https://doi.org/10.1128/JVI.77.5.3007-3019.2003.
64. Berger C, Romero-Brey I, Radujkovic D, Terreux R, Zayas M, Paul D, Harak C, Hoppe S, Gao M, Penin F, Lohmann V, Bartenschlager R. 2014. Daclatasvir-like inhibitors of NS5A block early biogenesis of hepatitis C virus-induced membranous replication factories, independent of RNA replication. Gastroenterology 147:1094–1105. https://doi.org/10.1053/j.gastro.2014.07.019.
65. Backes P, Quinkert D, Reiss S, Binder M, Zayas M, Rescher U, Gerke V, Bartenschlager R, Lohmann V. 2010. Role of annexin A2 in the production of infectious hepatitis C virus particles. J Virol 84:5775–5789. https://doi.org/10.1128/JVI.02343-09.
66. Lohmann V, Korner F, Koch J, Herian U, Theilmann L, Bartenschlager R. 1999. Replication of subgenomic hepatitis C virus RNAs in a hepatoma cell line. Science 285:110–113. https://doi.org/10.1126/science.285.5424.110.
67. Pietschmann T, Kaul A, Koutsoudakis G, Shavinskaya A, Kallis S, Steinmann E, Abid K, Negro F, Dreux M, Cosset FL, Bartenschlager R. 2006. Construction and characterization of infectious intragenotypic and intergenotypic hepatitis C virus chimeras. Proc Natl Acad Sci U S A 103:7408–7413. https://doi.org/10.1073/pnas.0504877103.
68. Wakita T, Pietschmann T, Kato T, Date T, Miyamoto M, Zhao Z, Murthy K, Habermann A, Krausslich HG, Mizokami M, Bartenschlager R, Liang TJ. 2005. Production of infectious hepatitis C virus in tissue culture from a cloned viral genome. Nat Med 11:791–796. https://doi.org/10.1038/nm1268.
69. Yi M, Lemon SM. 2004. Adaptive mutations producing efficient replication of genotype 1a hepatitis C virus RNA in normal Huh7 cells. J Virol 78:7904–7915. https://doi.org/10.1128/JVI.78.15.7904-7915.2004.
70. Saeed M, Scheel TK, Gottwein JM, Marukian S, Dustin LB, Bukh J, Rice CM. 2012. Efficient replication of genotype 3a and 4a hepatitis C virus replicons in human hepatoma cells. Antimicrob Agents Chemother 56:5365–5373. https://doi.org/10.1128/AAC.01256-12.
71. Fischl W, Bartenschlager R. 2013. High-throughput screening using dengue virus reporter genomes. Methods Mol Biol 1030:205–219. https://doi.org/10.1007/978-1-62703-484-5_17.
72. Kaul A, Stauffer S, Berger C, Pertel T, Schmitt J, Kallis S, Zayas M, Lohmann V, Luban J, Bartenschlager R. 2009. Essential role of cyclophilin A for hepatitis C virus replication and virus production and possible link to polyprotein cleavage kinetics. PLoS Pathog 5:e1000546. https://doi.org/10.1371/journal.ppat.1000546.
73. Klages N, Zufferey R, Trono D. 2000. A stable system for the high-titer

production of multiply attenuated lentiviral vectors. Mol Ther 2:170–176. https://doi.org/10.1006/mthe.2000.0103.
74. van den Hoff MJ, Moorman AF, Lamers WH. 1992. Electroporation in 'intracellular' buffer increases cell survival. Nucleic Acids Res 20:2902. https://doi.org/10.1093/nar/20.11.2902.
75. Linder MD, Uronen RL, Holtta-Vuori M, van der Sluijs P, Peranen J, Ikonen E. 2007. Rab8-dependent recycling promotes endosomal cholesterol removal in normal and sphingolipidosis cells. Mol Biol Cell 18:47–56. https://doi.org/10.1091/mbc.E06-07-0575.
76. Rieber N, Knapp B, Eils R, Kaderali L. 2009. RNAither, an automated pipeline for the statistical analysis of high-throughput RNAi screens. Bioinformatics 25:678–679. https://doi.org/10.1093/bioinformatics/btp014.
77. Kärber G. 1931. Beitrag zur kollektiven Behandlung pharmakologischer Reihenversuche. Arch Exp Pathol Pharmakol 162:480–487. https://doi.org/10.1007/BF01863914.
78. Spearman C. 1908. The method of 'right and wrong cases' ('constant stimuli') without Gauss's formulae. Br J Psychol 2:227–242.
79. Steinmann E, Brohm C, Kallis S, Bartenschlager R, Pietschmann T. 2008. Efficient trans-encapsidation of hepatitis C virus RNAs into infectious virus-like particles. J Virol 82:7034–7046. https://doi.org/10.1128/JVI.00118-08.
80. Soccio RE, Breslow JL. 2004. Intracellular cholesterol transport. Arterioscler Thromb Vasc Biol 24:1150–1160. https://doi.org/10.1161/01.ATV.0000131264.66417.d5.